

**Wild Bootstrap Inference for Non-Negative Matrix Factorization with Random
Effects**

Kenichi Satoh

Faculty of Data Science

Shiga University

arXiv:2603.01468v1 [stat.ME] 2 Mar 2026

Author Note

Kenichi Satoh  <https://orcid.org/0000-0003-4436-9347>

Correspondence concerning this article should be addressed to Kenichi Satoh,
Faculty of Data Science, Shiga University, Banba 1-1-1, Hikone, Shiga 522-8522, Japan.

E-mail: kenichi-satoh@biwako.shiga-u.ac.jp

The author declares no competing interests.

Abstract

Non-negative matrix factorization (NMF) is widely used for parts-based representations, yet formal inference for covariate effects is rarely available when the basis is learned under non-negativity. We introduce non-negative matrix factorization with random effects (NMF-RE), a mean-structure latent-variable model $Y = X(\Theta A + U) + \mathcal{E}$ that combines covariate-driven scores with unit-specific deviations. Random effects act as a working device for modeling heterogeneity and controlling complexity; we monitor their effective degrees of freedom and enforce a df-based cap to prevent near-saturated fits. Estimation alternates closed-form ridge (BLUP-like) updates for U with multiplicative non-negative updates for X and Θ . For inference on Θ , we condition on $(\widehat{X}, \widehat{U})$ and obtain fast uncertainty quantification via asymptotic linearization, a one-step Newton update, and a multiplier (wild) bootstrap; this avoids repeated constrained re-optimization. Simulations include a targeted stress test showing that, without df control, the random-effects penalty can collapse and inference for Θ becomes degenerate, whereas the df-cap prevents this failure mode. The non-negativity constraint induces sparse, parts-based loadings—a measurement-side variable selection—while inference on Θ identifies which covariates affect which components, providing covariate-side selection. Longitudinal, psychometric, spatial-flow, and text examples further illustrate stable, interpretable covariate-effect inference.

Keywords: Non-negative matrix factorization (NMF), Random effects, Variable selection, Effective degrees of freedom, Post-regularization inference, Wild bootstrap

Wild Bootstrap Inference for Non-Negative Matrix Factorization with Random Effects

1 Introduction

Non-negative matrix factorization (NMF) produces an interpretable, parts-based representation of multivariate non-negative data and is now routine in text analysis, image processing, topic modeling, and genomics (Cemgil, 2009; D. Lee & Seung, 2000; D. D. Lee & Seung, 1999; Schmidt et al., 2009). Beyond its algorithmic appeal, NMF admits a statistical interpretation as a latent-variable model specified through a *reconstruction (mean) structure*: each observation is approximated by an additive combination of non-negative basis profiles and latent scores. This emphasis on mean structure contrasts with classical factor analysis and structural equation models (SEM), which are commonly formulated through covariance structures (Bollen, 1989; Jöreskog & Goldberger, 1975).

Mean-structure modeling has a long tradition in longitudinal and psychometric research, where growth-curve models represent repeated measurements via regression on a prespecified design matrix (Laird & Ware, 1982; Potthoff & Roy, 1964; Satoh & Yanagihara, 2010; Vonesh & Carter, 1987).

From this perspective, NMF can be viewed as a *data-adaptive* analogue of mean-structure models: the basis matrix plays the role of a design matrix, but is *learned* from the data under non-negativity constraints rather than fixed a priori.

Bayesian and probabilistic formulations make this data-adaptive view explicit by casting NMF as a latent-variable model with working likelihoods and priors (Cemgil, 2009; Schmidt et al., 2009), and statistical NMF has been developed for count data and model selection in genomics and related settings (Rosales et al., 2017).

Covariate-aware Bayesian NMF extensions have been developed for specific likelihood settings, notably count-based mutational-signature models (Grabski et al., 2025; Robinson et al., 2019). In a frequentist direction, Phelan and Campbell (2025) recently combined separable (convex) NMF with post-hoc regression and nonparametric bootstrap

for topic models; their two-stage approach fixes the basis and regresses topic proportions on covariates, but does not incorporate random effects or enforce non-negativity on the covariate-effect matrix. Despite this growing statistical literature, comparatively little attention has been paid to *joint* frequentist inference that integrates covariate effects, unit-level random effects, and non-negativity constraints within a single estimation and bootstrap framework. Our focus is on this gap: optimization-based inference with explicit complexity diagnostics for random effects.

A natural way to incorporate covariates is to replace free scores with a regression $B = \Theta A$, yielding the covariate-driven approximation $Y \approx X\Theta A$ with the “design” matrix X learned under non-negativity (Ding et al., 2006; Satoh, 2023). This formulation entails an implicit form of *variable selection*: the non-negativity and low-rank constraints on X jointly induce sparse, parts-based loadings, so that each component retains only those observed variables that contribute to it—a measurement-side selection achieved without an explicit sparsity penalty. When effects of covariates on latent scores in Θ are subjected to formal inference, the resulting significance tests further identify which covariates affect which components, providing a complementary covariate-side selection.

When Θ is the parameter of scientific interest, formal inference is essential; yet covariance-centric modeling becomes fragile when P is moderate to large. We therefore extend covariate-driven NMF by introducing unit-specific random effects, leading to *NMF with random effects* (NMF-RE):

$$Y = X(\Theta A + U) + \mathcal{E}, \quad \mathbf{y}_n = X(\Theta \mathbf{a}_n + \mathbf{u}_n) + \boldsymbol{\varepsilon}_n.$$

Here X is a shared non-negative basis matrix, Θ captures systematic covariate effects on latent scores, U contains unit-specific deviations in the latent score space, and \mathcal{E} is an error matrix. This parallels mixed-effects modeling (Breslow & Clayton, 1993; Kenward & Roger, 1997; Laird & Ware, 1982), but differs fundamentally in that the basis X is unknown and estimated under non-negativity constraints. We therefore view NMF-RE as a mixed-effects latent-variable model defined on a reconstruction (mean) structure rather

than on a covariance structure.

Weakly regularized random effects can absorb idiosyncratic variation and destabilize inference for Θ (Efron, 2004; Tibshirani & Taylor, 2012). We therefore treat $\lambda = \sigma^2/\tau^2$ as a complexity-control device and explicitly monitor the effective degrees of freedom consumed by U .

Estimation uses a block-wise scheme: random effects are updated via ridge-type BLUP-like closed forms, while X and Θ are updated via non-negative multiplicative rules. To prevent near-saturated regimes, we impose a diagnostic cap on the effective degrees of freedom of U ; the cap is a numerical safeguard and is inactive under regular operating conditions.

Statistical inference targets Θ and is conducted *conditional on the estimated regularized solution* $(\widehat{X}, \widehat{U})$. Adopting a post-regularization perspective (Javanmard & Montanari, 2014; van de Geer et al., 2014), we avoid repeated constrained re-optimization by combining (i) asymptotic linearization, (ii) a one-step Newton update, and (iii) a multiplier (wild) bootstrap based on weighted score contributions. This yields computationally efficient uncertainty quantification compatible with the algorithmic structure of NMF.

Our main contributions are:

1. We propose NMF-RE, a mean-structure formulation of covariate-driven NMF with unit-specific random effects under non-negativity constraints.
2. We introduce an effective-degrees-of-freedom diagnostic for the random effects and a df-based cap that prevents near-saturated regimes.
3. We develop post-regularization inference for Θ via the above three-step strategy, avoiding repeated constrained optimization.
4. Through simulations (including a targeted stress test of the dfU-cap) and four empirical studies, we demonstrate stable inference across longitudinal, psychometric,

spatial-flow, and text-analysis settings. The empirical illustrations show that the learned \widehat{X} achieves measurement-side variable selection—grouping observed variables into interpretable components without a prespecified loading pattern—while inference on Θ provides covariate-side variable selection by identifying which covariates significantly affect which components.

More broadly, this work advocates a mean-structure-centric approach to inference in constraint-based latent-variable models, combining interpretable reconstruction structures, explicit complexity control, and implicit variable selection through non-negative latent structure.

2 Model

2.1 Data structure and notation

Let $Y \in \mathbb{R}_{\geq 0}^{P \times N}$ be a non-negative data matrix with P observed variables (items, words, regions, ages) and N units (subjects, documents, origin–destination nodes). Let $A \in \mathbb{R}^{K \times N}$ collect observed covariates for the N units, with n th column $\mathbf{a}_n \in \mathbb{R}^K$. We write $\mathbf{1}_m$ for an m -vector of ones and use Q for the target latent dimension (rank).

Coding of covariates. Because we impose elementwise non-negativity on the covariate-effect matrix Θ (Section 2.2), it is convenient to code covariates so that A is entrywise non-negative (e.g., intercepts, indicators, and non-negative rescalings). When a covariate takes both signs, we use the standard positive/negative-part expansion $a = a^+ - a^-$ with $a^+ = \max(a, 0)$ and $a^- = \max(-a, 0)$, and include both a^+ and a^- as separate non-negative covariates. This preserves $\Theta \geq 0$ without restricting the class of linear effects representable by ΘA .

2.2 NMF with covariates

Classical NMF approximates Y by a low-rank non-negative product $Y \approx XB$, where $X \in \mathbb{R}_{\geq 0}^{P \times Q}$ is a basis matrix and $B \in \mathbb{R}_{\geq 0}^{Q \times N}$ is a score (coefficient) matrix (Gillis, 2014, 2020; D. Lee & Seung, 2000; D. D. Lee & Seung, 1999). To incorporate observed

covariates, we parameterize the scores by a regression on A ,

$$B = \Theta A, \quad (1)$$

where $\Theta \in \mathbb{R}_{\geq 0}^{Q \times K}$ represents covariate effects on latent scores. The resulting reconstruction (mean) structure is

$$Y \approx X\Theta A,$$

which is formally analogous to the mean structure of growth-curve models (Laird & Ware, 1982; Potthoff & Roy, 1964; Satoh & Yanagihara, 2010; Vonesh & Carter, 1987), with the key distinction that X is *learned* under non-negativity constraints rather than fixed as a prespecified design matrix. Related tri-factor representations appear in the machine-learning literature (Ding et al., 2006), but here we emphasize regression-style interpretation with Θ as the primary parameter of interest.

2.3 NMF with random effects (NMF-RE)

In many longitudinal and multilevel settings, observed covariates do not fully explain unit-to-unit heterogeneity. To capture unexplained deviations while preserving interpretability, we propose NMF with random effects (NMF-RE):

$$Y = X(\Theta A + U) + \mathcal{E}, \quad (2)$$

where $X \in \mathbb{R}_{\geq 0}^{P \times Q}$ is a shared non-negative basis, $\Theta \in \mathbb{R}_{\geq 0}^{Q \times K}$ is a non-negative covariate-effect matrix, $U \in \mathbb{R}^{Q \times N}$ is a matrix of unit-specific random effects, and $\mathcal{E} \in \mathbb{R}^{P \times N}$ is an error matrix.

We treat A as fixed (nonrandom) throughout. Randomness is attributed to U and \mathcal{E} , and hence to Y through (2). We adopt the following working moment structure:

$$E(\text{vec}(\mathcal{E})) = \mathbf{0}_{PN}, \quad E(\text{vec}(U)) = \mathbf{0}_{QN}, \quad (3)$$

$$\text{Var}(\text{vec}(\mathcal{E})) = \sigma^2 I_{PN}, \quad \text{Var}(\text{vec}(U)) = \tau^2 I_{QN}, \quad (4)$$

$$\text{Cov}(\text{vec}(U), \text{vec}(\mathcal{E})) = \mathbf{0}_{QN \times PN}. \quad (5)$$

Under these working assumptions,

$$\text{Var}(\mathbf{y}_n \mid \mathbf{a}_n) = \tau^2 X X^\top + \sigma^2 I_P, \quad (6)$$

highlighting the connection to linear mixed-effects models while keeping the focus on the reconstruction (mean) structure.

Unit-level interpretation. For unit n ,

$$\mathbf{y}_n = X(\Theta \mathbf{a}_n + \mathbf{u}_n) + \boldsymbol{\varepsilon}_n, \quad (7)$$

where \mathbf{a}_n is fixed, while \mathbf{u}_n and $\boldsymbol{\varepsilon}_n$ are random. Thus, columns of X define Q shared non-negative latent profiles, the term $\Theta \mathbf{a}_n$ describes systematic covariate modulation of latent scores, and \mathbf{u}_n captures idiosyncratic departures. This constitutes the mean-structure perspective introduced above, complementing covariance-based SEM formulations (Bollen, 1989; Jöreskog, 1969; Jöreskog & Goldberger, 1975). As special cases, NMF-RE reduces to random-coefficient growth-curve models when X is known (Laird & Ware, 1982; Potthoff & Roy, 1964; Satoh & Yanagihara, 2010), and to standard NMF when A is absent or U is suppressed (D. Lee & Seung, 2000; Schmidt et al., 2009).

Remark on signs and constraints. We impose $X \geq 0$ and $\Theta \geq 0$ for interpretability, but allow U to be real-valued; ridge regularization and df-monitoring (Sections 3–3.4) prevent near-saturated behavior.

2.4 Constraints, normalization, and identifiability

NMF-type models are not fully identifiable because $X(\Theta A + U)$ is invariant under $X \leftarrow X D^{-1}$ and $(\Theta, U) \leftarrow (D\Theta, DU)$ for any diagonal matrix D with positive diagonal entries, and under permutation of latent components. To fix scale, we impose a normalization on X . In our implementation we use the column-sum constraint

$$X \geq 0, \quad \Theta \geq 0, \quad \mathbf{1}_P^\top X = \mathbf{1}_Q^\top, \quad (8)$$

and absorb the induced scaling into Θ (and into U when needed). This normalization preserves interpretability: each column of X can be viewed as a non-negative profile (e.g., a distribution over variables), while rows of ΘA provide the component scales across units.

Beyond scale and permutation indeterminacy, NMF generally admits only partial identifiability; nevertheless, normalization and non-negativity often yield stable and interpretable decompositions in practice (Gillis, 2014, 2020; Gillis & Rajkó, 2023).

3 Estimation

3.1 Complexity control via the random-effects penalty

We treat τ^2 primarily as a complexity-control parameter: $\lambda = \sigma^2/\tau^2$ governs the permitted unit-specific deviation. Large τ^2 (small λ) allows near-saturated fits; small τ^2 shrinks U toward zero. This motivates explicit monitoring of the effective degrees of freedom consumed by U (Section 3.4) and a diagnostic cap (Section 3.5).

3.2 Working objective

Based on the model in Section 2, we estimate (X, Θ, U) by minimizing the penalized least-squares criterion

$$\mathcal{L}(X, \Theta, U) = \|Y - X(\Theta A + U)\|_F^2 + \lambda \|U\|_F^2, \quad (9)$$

subject to

$$X \geq 0, \quad \Theta \geq 0, \quad \mathbf{1}_P^\top X = \mathbf{1}_Q^\top.$$

Here $\|\cdot\|_F$ is the Frobenius norm and λ is the complexity-control penalty introduced in Section 3.1. We use (9) as a *working* objective for computation; formal inference for Θ is developed in Section 4.

3.3 Block-wise estimation scheme

Joint minimization of (9) under non-negativity constraints is computationally challenging. We therefore adopt a block-wise scheme that alternates updates for U , X , and Θ , holding the remaining blocks fixed. This preserves the structure of classical NMF algorithms (Févotte & Idier, 2011; D. Lee & Seung, 2000) while incorporating random effects.

3.3.1 *U-step: ridge-type update*

With X and Θ fixed, define $B = \Theta A$. The U -subproblem is

$$\min_U \|Y - X(B + U)\|_F^2 + \lambda \|U\|_F^2.$$

This decouples across units. For the n th column,

$$\mathbf{u}_n = (X^\top X + \lambda I_Q)^{-1} X^\top (\mathbf{y}_n - X \mathbf{b}_n), \quad (10)$$

where \mathbf{y}_n and \mathbf{b}_n are the n th columns of Y and B , respectively. Equation (10) is a ridge-type update analogous to BLUP-like random effects estimators in linear mixed-effects models (Breslow & Clayton, 1993; Laird & Ware, 1982). After updating U , we center each row to enforce zero mean across units, which improves identifiability by preventing systematic offsets from being absorbed by U .

Computation. For fixed X and λ , the matrix $(X^\top X + \lambda I_Q)^{-1} X^\top$ is common to all columns, so the U -update can be implemented efficiently by forming and reusing the $Q \times Q$ solve.

3.3.2 *X-step: multiplicative non-negative update*

With Θ and U fixed, define

$$B_U = \Theta A + U.$$

Because U is real-valued, B_U may contain negative entries. To preserve the non-negativity and numerical stability of multiplicative updates, we use the elementwise positive part

$$B_U^+ = \max(B_U, 0)$$

as a stabilized surrogate in the update below. We update X using a Euclidean multiplicative rule,

$$X \leftarrow X \odot \left(Y (B_U^+)^{\top} \right) \oslash \left(X (B_U^+ (B_U^+)^{\top}) \right), \quad (11)$$

where \odot and \oslash denote Hadamard product and division, respectively.

Normalization. After the update, we renormalize columns of X to satisfy $\mathbf{1}_P^\top X = \mathbf{1}_Q^\top$. If $X \leftarrow XD^{-1}$ is the normalization, we apply the corresponding scaling $(\Theta, U) \leftarrow (D\Theta, DU)$ so that the fitted mean $X(\Theta A + U)$ is unchanged (Section 2.4).

Remark. When $U \equiv 0$ (or $B_U \geq 0$), (11) reduces to the standard Euclidean multiplicative update (Févotte & Idier, 2011; D. Lee & Seung, 2000). The positive-part stabilization is introduced solely to keep the multiplicative scheme well-defined when U is real-valued; we monitor the working objective (9) to ensure stable descent in practice.

3.3.3 Θ -step: covariate-driven update

With X and U fixed, Θ is updated by minimizing

$$\|Y - X(\Theta A + U)\|_F^2 \quad \text{subject to } \Theta \geq 0.$$

Let $Y_U = Y - XU$. Because Y_U may have negative entries, we use the positive part $Y_U^+ = \max(Y_U, 0)$ to obtain a stable multiplicative update,

$$\Theta \leftarrow \Theta \odot \left(X^\top Y_U^+ A^\top \right) \oslash \left((X^\top X \Theta)(A A^\top) \right). \quad (12)$$

This is a covariate-adapted version of multiplicative updates for non-negative tri-factorization (Ding et al., 2006), stabilized for real-valued U .

3.4 Effective degrees of freedom of U

The ridge update (10) introduces additional model flexibility. For fixed X and λ , the fitted random-effects contribution can be written using the ridge “hat” matrix

$$H_\lambda = X(X^\top X + \lambda I_Q)^{-1} X^\top.$$

We define the effective degrees of freedom consumed by U as

$$\text{df}_U = N \text{tr}(H_\lambda). \quad (13)$$

Let d_1, \dots, d_Q be the eigenvalues of $X^\top X$. Then $\text{tr}(H_\lambda) = \sum_{q=1}^Q d_q / (d_q + \lambda)$ and hence

$$\text{df}_U = N \sum_{q=1}^Q \frac{d_q}{d_q + \lambda}, \quad (14)$$

which matches the classical ridge-regression degrees-of-freedom expression and connects directly to complexity measures in penalized estimation (Efron, 2004; Tibshirani & Taylor, 2012). This representation is convenient because df_U is monotone decreasing in λ for fixed X , enabling simple one-dimensional control.

3.5 Diagnostic control via a dfU-cap

To avoid near-saturated regimes in which U absorbs most idiosyncratic variation, we impose a diagnostic cap

$$df_U(\lambda) \leq df_U^{\max}.$$

Because $df_U(\lambda)$ is monotone decreasing in λ (Section 3.4), we define

$$\lambda_{\text{cap}}(X) = \inf\{\lambda > 0 : df_U(\lambda) \leq df_U^{\max}\}.$$

Whenever the current λ violates the cap, we enforce

$$\lambda \leftarrow \max\{\lambda, \lambda_{\text{cap}}(X)\},$$

holding X fixed, and use this enforced value in the subsequent U -update. Because the mapping $\lambda \mapsto df_U(\lambda)$ is monotone, $\lambda_{\text{cap}}(X)$ can be obtained efficiently by a one-dimensional search (e.g., bisection using the eigenvalue form (14)).

Interpretation and practical calibration. The dfU-cap is a numerical safeguard, not a tuning parameter for prediction. In practice, the cap ratio $r^{\max} = df_U^{\max}/(NQ)$ is calibrated by translating an analyst-imposed lower bound on λ into an implied saturation level via the eigenvalues of $X_{\text{fix}}^{\top}X_{\text{fix}}$, where X_{fix} is obtained from the initialization fit with $U \equiv 0$ (details in Appendix A). For transparent reporting, we distinguish whether the cap was ever *activated* during optimization and whether the final solution is *binding* ($df_U = df_U^{\max}$) or non-binding.

3.6 Convergence, initialization, and implementation

The block-wise updates are iterated until the relative change in the working objective (9) falls below a tolerance. A typical iteration proceeds as follows: (i) enforce the

dfU-cap at the current X (Section 3.5); (ii) update U by (10) and row-center; (iii) update X by (11) and renormalize, applying the induced scaling to (Θ, U) ; (iv) update Θ by (12).

Initialization uses a covariate-driven NMF fit (with $U \equiv 0$) to obtain starting values for (X, Θ) , after which U is introduced and updated by ridge steps. All updates admit closed-form or multiplicative expressions and scale to moderate and large matrices.

Working scale used during optimization. In some implementations we update a working scale to stabilize the effective penalty level, using $\hat{\sigma}_{\text{iter}}^2 = \|R\|_F^2 / (PN)$ with $R = Y - X(\Theta A + U)$, and expressing λ through $\hat{\sigma}_{\text{iter}}^2$ when needed. This iteration-scale quantity is used only for numerical stabilization; for statistical inference we instead use a degrees-of-freedom adjusted variance estimator (Section 4.2).

A reference implementation is available in the `nmfkc` package (Satoh, 2025), and all scripts needed to reproduce the numerical results in this paper are provided at <https://github.com/ksatohds/nmfre-paper>. The complete block-wise estimation algorithm, including pseudocode for all steps and the descent safeguard, is given in Appendix B.

Variable selection as an estimation outcome. The non-negativity and low-rank constraints on X are not designed as explicit sparsity penalties, yet the estimated \widehat{X} typically exhibits sparse, parts-based structure in which each component loads on only a subset of observed variables—an implicit measurement-side variable selection that emerges from the estimation procedure. When combined with formal inference for Θ (Section 4), significance testing further identifies which covariates affect which components, providing a complementary covariate-side selection.

4 Inference

4.1 Scope and inferential target

This section develops statistical inference for the covariate-effect matrix Θ in the NMF-RE model. Our inferential target is Θ *conditional on* the estimated regularized representation $(\widehat{X}, \widehat{U})$ obtained in Section 3, in the spirit of post-regularization inference (Javanmard & Montanari, 2014; Taylor & Tibshirani, 2015; van de Geer et al., 2014).

Robustness to working-model misspecification is pursued via sandwich and multiplier bootstrap constructions.

4.2 Profiled score, information, and variance scale

Let \widehat{X} denote the estimated basis matrix from Section 3, and let λ denote the final ridge penalty used for the random effects. For inference on Θ , we treat (\widehat{X}, λ) as fixed and profile out U via ridge regression for each candidate Θ :

$$\widehat{U}(\Theta) = \arg \min_{U \in \mathbb{R}^{Q \times N}} \|Y - \widehat{X}(\Theta A + U)\|_F^2 + \lambda \|U\|_F^2.$$

This yields the column-wise update

$$\widehat{\mathbf{u}}_n(\Theta) = (\widehat{X}^\top \widehat{X} + \lambda I_Q)^{-1} \widehat{X}^\top (\mathbf{y}_n - \widehat{X} \Theta \mathbf{a}_n), \quad n = 1, \dots, N,$$

which coincides with \widehat{U} at $\Theta = \widehat{\Theta}$.

Variance scale. We treat σ^2 as a nuisance scale and use a degrees-of-freedom adjusted estimator

$$\widehat{\sigma}^2 = \frac{\|Y - \widehat{X}(\widehat{\Theta} A + \widehat{U})\|_F^2}{PN - \text{df}_U - \text{df}_\Theta}, \quad (15)$$

where df_U is the effective degrees of freedom consumed by the ridge random-effects update under (\widehat{X}, λ) (Section 3.4). For Θ , a simple working choice is $\text{df}_\Theta = QK$. Because $\Theta \geq 0$ may place some coefficients on the boundary, a more boundary-aware alternative is to use an “active-set” degrees of freedom

$$\text{df}_\Theta^{\text{act}} = \#\{(q, k) : \widehat{\Theta}_{qk} > \delta\},$$

with a small tolerance $\delta > 0$ (e.g., $\delta = 10^{-8}$ times a scale factor). In our experiments, the difference between QK and $\text{df}_\Theta^{\text{act}}$ was typically small; we report which convention is used. In all subsequent expressions, σ^2 is replaced by its plug-in estimate $\widehat{\sigma}^2$.

Profiled residual and score contributions. Let

$$\mathbf{r}_n(\Theta) = \mathbf{y}_n - \widehat{X}(\Theta \mathbf{a}_n + \widehat{\mathbf{u}}_n(\Theta))$$

denote the profiled residual for unit n . Differentiating the profiled objective with respect to Θ and using the first-order optimality of $\widehat{\mathbf{u}}_n(\Theta)$ (envelope theorem) yields the score contribution

$$S_n(\Theta) = -\frac{1}{\sigma^2} \left(\widehat{X}^\top \mathbf{r}_n(\Theta) \right) \mathbf{a}_n^\top, \quad n = 1, \dots, N. \quad (16)$$

We use $\text{vec}(\cdot)$ to denote column-stacking vectorization; inference targets $\text{vec}(\Theta) \in \mathbb{R}^{QK}$.

Ridge hat matrix and shrinkage representation. Define the ridge hat matrix in the \widehat{X} -space,

$$H_\lambda = \widehat{X}(\widehat{X}^\top \widehat{X} + \lambda I_Q)^{-1} \widehat{X}^\top.$$

Substituting the ridge update into the residual shows that

$$\mathbf{r}_n(\Theta) = (I_P - H_\lambda) \left(\mathbf{y}_n - \widehat{X} \Theta \mathbf{a}_n \right),$$

so profiling out U shrinks variation in the \widehat{X} -space through $(I_P - H_\lambda)$.

Working information. If one ignores the effect of profiling out U when forming curvature with respect to Θ , a Fisher-type working information matrix is

$$\mathcal{I}_0(\Theta) = \frac{1}{\sigma^2} \left(A A^\top \otimes \widehat{X}^\top \widehat{X} \right). \quad (17)$$

Information reduction due to profiling out U . Profiling out U reduces the effective information for Θ :

$$\mathcal{I}(\Theta) = \frac{1}{\sigma^2} \left(A A^\top \otimes \left(\widehat{X}^\top (I_P - H_\lambda) \widehat{X} \right) \right), \quad (18)$$

where the inner matrix simplifies to $\lambda \widehat{X}^\top \widehat{X} (\widehat{X}^\top \widehat{X} + \lambda I_Q)^{-1}$. We use (18) evaluated at $\widehat{\Theta}$.

4.3 Sandwich covariance estimation

Because the Gaussian working model may be misspecified, we employ a sandwich-type covariance estimator based on score contributions. Let

$$\widehat{\mathcal{I}} = \mathcal{I}(\widehat{\Theta}), \quad \widehat{\mathcal{J}} = \sum_{n=1}^N \text{vec} \left(S_n(\widehat{\Theta}) \right) \text{vec} \left(S_n(\widehat{\Theta}) \right)^\top.$$

The sandwich covariance estimator for $\text{vec}(\widehat{\Theta})$ is

$$\widehat{\text{Var}} \left(\text{vec}(\widehat{\Theta}) \right) = \widehat{\mathcal{I}}^{-1} \widehat{\mathcal{J}} \widehat{\mathcal{I}}^{-1}. \quad (19)$$

Finite-sample corrections (e.g., HC-type scaling) and cluster-robust variants may be applied when unit-level score contributions exhibit heteroskedasticity or within-cluster dependence (Cameron et al., 2008).

4.4 One-step Newton approximation

Direct bootstrap inference would require repeated re-optimization under non-negativity constraints, which is computationally expensive. Instead, we approximate bootstrap replicates by a one-step Newton update around $\hat{\Theta}$:

$$\text{vec}(\hat{\Theta}^*) = \text{vec}(\hat{\Theta}) - \hat{\mathcal{I}}^{-1} S^*(\hat{\Theta}), \quad (20)$$

where $S^*(\hat{\Theta})$ denotes a resampled score vector. This construction exploits the asymptotic linearity of $\hat{\Theta}$ and is standard in post-regularization inference (Javanmard & Montanari, 2014; van de Geer et al., 2014).

Non-negativity in one-step replicates. Because (20) is an unconstrained linear update, the resulting $\hat{\Theta}^*$ may violate the elementwise constraint $\Theta \geq 0$, especially for coefficients near the boundary. In implementation, we apply the elementwise projection

$$\hat{\Theta}^* \leftarrow \max(\hat{\Theta}^*, 0)$$

when forming bootstrap replicates. For coefficients estimated at (or near) zero, boundary effects may induce non-Gaussian and truncated finite-sample behavior; in such cases, one-sided tests and percentile-type bootstrap summaries are typically more appropriate than two-sided Wald normal approximations (see Section 5).

The asymptotic justification of the one-step map—showing that (20) is asymptotically equivalent to the fully iterated Z-estimator in the interior regime under standard regularity conditions—is given in Appendix C (see also Huber et al., 1967; Javanmard & Montanari, 2014; Taylor & Tibshirani, 2015; van de Geer et al., 2014; White, 1980).

4.5 Multiplier (wild) bootstrap for score contributions

We generate resampled scores using a multiplier bootstrap scheme (often referred to as a wild bootstrap for estimating-equation contributions). Let ξ_1, \dots, ξ_N be i.i.d. multipliers with $E(\xi_n) = 0$ and $\text{Var}(\xi_n) = 1$, such as Rademacher (± 1), standard normal, or exponential-centered weights ($\xi_n = \zeta_n - 1$ with $\zeta_n \sim \text{Exp}(1)$) (Cameron et al., 2008; Mammen, 1993). In all experiments reported below, we use the exponential-centered distribution. We form the resampled score

$$S^*(\hat{\Theta}) = \sum_{n=1}^N \xi_n \text{vec}(S_n(\hat{\Theta})),$$

and substitute into (20) to obtain bootstrap replicates $\hat{\Theta}^*$ without re-solving the constrained optimization problem.

Bootstrap standard errors and confidence intervals for elements of Θ are computed from the empirical distribution of $\{\hat{\Theta}^*\}$. We report both sandwich-based standard errors and bootstrap-based standard errors to provide a transparent assessment of uncertainty and of the adequacy of the one-step approximation.

4.6 Computational notes

The Kronecker structure $\hat{\mathcal{L}} = \hat{\sigma}^{-2}(AA^\top \otimes F)$ with $F = \widehat{X}^\top(I_P - H_\lambda)\widehat{X} \in \mathbb{R}^{Q \times Q}$ allows the one-step update and sandwich covariance to be computed via small $K \times K$ and $Q \times Q$ inversions without forming the full $(QK) \times (QK)$ matrix.

4.7 Validity, scope, and practical diagnostics

The proposed inference targets Θ conditional on the selected regularized representation $(\widehat{X}, \widehat{U})$. Under standard regularity conditions for M/Z-estimators, the sandwich covariance estimator (19) provides large-sample robust standard errors even under a misspecified Gaussian working model, and the multiplier bootstrap combined with the one-step Newton map yields a computationally efficient resampling approximation (Cameron et al., 2008; Huber et al., 1967; van de Geer et al., 2014; White, 1980). Because bootstrap replicates are projected onto $\Theta \geq 0$, coefficients near the boundary may exhibit

truncation, so directional tests and percentile bootstrap summaries are recommended in boundary regimes. A detailed discussion of the inferential scope, regularity conditions, boundary behavior, and practical diagnostics (including recommended reporting items) is given in Appendix D.

5 Simulation study

5.1 Goal and design

This section evaluates the finite-sample behavior of the proposed *post-regularization* inference for the covariate-effect matrix Θ in NMF-RE. The inferential target is Θ *conditional on* the fitted low-rank representation $(\widehat{X}, \widehat{U})$. Because (i) estimation uses non-negativity constraints and (ii) inference is performed after a regularized fit, the main practical question is whether the local linearization underlying the one-step Newton approximation (Section 4.4) yields uncertainty quantification that behaves stably in finite samples. Accordingly, we examine (a) the agreement between sandwich-based standard errors (SE) and one-step multiplier-bootstrap standard errors (BSE), and (b) the size and coverage of Wald-type tests and confidence intervals, paying special attention to boundary behavior induced by $\Theta \geq 0$.

Orthodont-based baseline design ($P = 4, Q = 1$). The simulation design mirrors the Orthodont illustration in Section 6.1. We fix $P = 4$ time points and rank $Q = 1$. The basis vector is set to the estimated Orthodont profile

$$X_{\text{true}} = (0.2308, 0.2409, 0.2566, 0.2717)^\top, \quad \mathbf{1}_P^\top X_{\text{true}} = 1.$$

The covariate matrix is $A = (\mathbf{1}, \text{male})^\top \in \mathbb{R}^{2 \times N}$. For $N = 27$, the `male` indicator follows the Orthodont sample. For $N \in \{100, 200\}$, we generate `male` i.i.d. Bernoulli with success probability equal to the Orthodont male proportion.

Data are generated from the NMF-RE mechanism

$$Y = X_{\text{true}}(\Theta_{\text{true}}A + U) + \mathcal{E}, \tag{21}$$

where $U \in \mathbb{R}^{Q \times N}$ has i.i.d. $N(0, \tau^2)$ entries and $\mathcal{E} \in \mathbb{R}^{P \times N}$ has i.i.d. entries independent of U . We set $\sigma^2 = \tau^2 = 1$ and use the corresponding working penalty $\lambda = \sigma^2/\tau^2 = 1$ as the baseline regularization level.

Error distributions (robustness check). To probe sensitivity to non-Gaussian observation noise while keeping the variance matched to the working model, we vary only \mathcal{E} :

- **Gaussian:** $\varepsilon_{pn} \sim N(0, 1)$.
- **Centered exponential:** $\varepsilon_{pn} = \xi_{pn} - 1$ with $\xi_{pn} \sim \text{Exp}(1)$, so that $E(\varepsilon_{pn}) = 0$ and $\text{Var}(\varepsilon_{pn}) = 1$ but the noise is positively skewed.

Unless noted otherwise, random effects U are generated from the Gaussian model above; thus, this robustness check targets deviations from Gaussianity in the measurement error.

Boundary vs. interior regimes. We consider two scenarios:

- **Null (boundary null):** $\Theta_{\text{true}}[\text{male}] = 0$. Because $\Theta \geq 0$, this null lies on the boundary, producing a truncated finite-sample distribution for $\hat{\theta}_{\text{male}}$.
- **Alternative (interior alternative):** $\Theta_{\text{true}}[\text{male}] = 9.4285$, matching the Orthodox estimate in Table 2.

In both scenarios, $\Theta_{\text{true}}[\text{intercept}] = 90.502$.

Fitting and inference (baseline design). For each $N \in \{27, 100, 200\}$ and each error distribution, we generate $R = 1000$ Monte Carlo datasets. Each dataset is fitted by the block-wise NMF-RE algorithm in Section 3, using the dfU diagnostic cap with $\text{df}_U^{\text{max}}/(NQ) = 0.21$. We use the same convergence tolerance and objective monitoring/safeguards as in Section 3, and (when applicable) retain the best solution across multiple initializations to mitigate non-convexity.

Inference uses the reduced information (18), the sandwich covariance (19), and the one-step multiplier bootstrap (Sections 4.4–4.5) with $B = 1000$ resamples and projection onto $\Theta \geq 0$. For the boundary-null scenario (Null), hypothesis testing and reported p -values are computed one-sided, aligned with the constraint $\theta_{\text{male}} \geq 0$.

Variance scale and degrees-of-freedom convention. Throughout the simulation we estimate the variance scale by (15). For df_Θ we use $\text{df}_\Theta = QK$ (working choice); results were qualitatively unchanged when replacing this by an active-set degrees of freedom count (Section 4.2).

Additional stress test for random-effects saturation (dfU-cap necessity).

To explicitly verify that dfU-cap functions as a safety device against random-effects saturation, we run an additional targeted stress experiment in a more flexible setting ($P = 4$, $Q = 3$, $N = 100$), where the working random-effects penalty is intentionally weakened to promote near-saturation. Full design details and results are reported in Appendix E.

5.2 Evaluation metrics

We report Monte Carlo bias, standard deviation (SD), and RMSE for the male-effect estimator $\hat{\theta}_{\text{male}}$. We also report Monte Carlo averages of SE and BSE. For hypothesis testing, we use a Wald-type statistic based on either SE or BSE. For the boundary null (Null), the main procedure is the one-sided test $H_0 : \theta_{\text{male}} = 0$ vs. $H_1 : \theta_{\text{male}} > 0$.

For interval estimation, we report coverage of nominal 95% Wald intervals based on SE and BSE, and coverage of the 95% percentile interval constructed from the one-step multiplier-bootstrap replicates. We monitor random-effects saturation via $\text{df}_U/(NQ)$: in the baseline $Q = 1$ study we summarize the Monte Carlo mean of $\text{df}_U/(NQ)$, while in the targeted $Q = 3$ stress test we additionally report an upper-tail summary, $\text{dfU}_{0.99}$, the 99th percentile of $\text{df}_U/(NQ)$ over Monte Carlo runs.

5.3 Results

The full Monte Carlo results are reported in Table F1 (Appendix F). The simulation supports the central claim of this paper: *conditional* inference for Θ after a regularized NMF-RE fit can be made stable in a controlled low-rank setting. Under the Alternative (interior regime), SE and BSE are close and coverages approach nominal levels as N increases, confirming that the one-step linearization is adequate when coefficients are away

from the boundary. Under the Null (boundary regime), BSE is systematically smaller than SE due to projection onto $\Theta \geq 0$, but the one-sided rejection rates remain close to 5% and coverages are slightly conservative. Replacing Gaussian errors by centered exponential errors yields qualitatively similar patterns, suggesting robustness to moderate non-Gaussianity. A detailed interpretation is provided in Appendix F.

The stress test results (Appendix E) show that without dfU-cap, the fitted penalty collapses ($\hat{\lambda} \approx 0$) and inference for Θ becomes degenerate, whereas a strict cap prevents this collapse and, under the Null, maintains near-nominal size and coverage. (Under the Alternative the intentionally weak initial penalty combined with the higher-dimensional random-effects space induces substantial bias in $\hat{\Theta}$ under all cap settings; this is expected for a stress scenario designed to probe failure modes rather than routine performance.) In the baseline $Q = 1$ design, the mean saturation ratio $\text{df}_U/(NQ)$ stays near 0.20 under the default cap $\text{df}_U^{\text{max}}/(NQ) = 0.21$, indicating that U is kept in a moderately regularized regime.

6 Empirical illustrations

We illustrate NMF-RE with four empirical examples of increasing complexity: Orthodont growth data, Holzinger–Swineford cognitive tests, origin–destination flows (OD–HUB), and a topic model. Table 1 provides a diagnostic summary of model sizes and the random-effects operating regime. The saturation ratio $r = \text{df}_U/(NQ)$ measures random-effects flexibility (0 = strongly regularized; 1 = near-saturated); the cap ratio $r^{\text{max}} = \text{df}_U^{\text{max}}/(NQ)$ is calibrated as in Section 3.5 (see also Appendix A). All reported solutions are non-binding ($\text{df}_U < \text{df}_U^{\text{max}}$).

In subsequent subsections, we report inference for Θ and interpret the estimated components in light of both the learned profiles (X) and the saturation diagnostics (r, r^{max}) .

Table 1

Summary of model sizes and random-effects magnitude across empirical examples. Here N is the number of units, P the number of observed variables, Q the latent dimension, and NQ the total number of random-effects entries. We report df_U and the saturation ratio $r = \text{df}_U/(NQ)$, together with the cap ratio $r^{\max} = \text{df}_U^{\max}/(NQ)$ used for the df_U -cap (Section 3.5). The column “Cap” indicates whether the df_U -cap was ever triggered during optimization, and λ is the final (possibly enforced) ridge penalty used in the reported fit.

Dataset	N	P	Q	NQ	df_U	r	r^{\max}	λ	Cap
Orthodont	27	4	1	27	5.42	0.201	0.21	1.00	No
HS1939	300	9	3	900	861.93	0.958	0.96	0.0104	No
OD-HUB	47	43	4	188	2.38	0.013	0.02	6.75	Yes
Topic model	59	67	3	177	1.30	0.007	0.02	3.30	Yes

6.1 Orthodont growth data

The Orthodont growth data consist of pituitary–pterygomaxillary fissure distances for $N = 27$ children (16 males, 11 females) at ages 8, 10, 12, and 14 (Laird & Ware, 1982; Pinheiro et al., 2025; Potthoff & Roy, 1964), yielding $P = 4$ repeated measurements with covariate $\mathbf{a}_n = (1, \text{male}_n)^\top$.

Benchmark: linear mixed-effects modeling (LMM). As an orientation benchmark, we also fitted a standard LMM with random intercept and slope (see Appendix G for details). The LMM confirms that the Orthodont data exhibit both substantial subject-level heterogeneity and sex-dependent mean structure, including a significant sex difference at age 11 and a sex-dependent growth rate.

NMF-RE specification ($Q = 1$). With $Q = 1$, the NMF-RE mean structure reduces to $\mathbf{y}_n = \mathbf{x}(\theta_0 + \theta_{\text{male}}\text{male}_n + u_n) + \boldsymbol{\varepsilon}_n$ with $\mathbf{x} \geq 0$, $\mathbf{1}_P^\top \mathbf{x} = 1$; here \mathbf{x} is a non-negative trajectory shape learned from the data.

Estimated basis profile and fitted curves. For $Q = 1$, the estimated basis vector \widehat{X} assigns non-negative weights to ages 8, 10, 12, and 14 years:

$$\widehat{X} = (0.2308, 0.2409, 0.2566, 0.2717)^\top, \quad \mathbf{1}_p^\top \widehat{X} = 1.$$

The increasing pattern indicates that the learned trajectory places progressively more mass on later ages, consistent with monotone growth. Figure 1 displays the observed measurements together with two fitted curves for each subject: the fixed-effects component $\widehat{X}\widehat{\Theta}\mathbf{a}_n$ and the BLUP-based fit $\widehat{X}(\widehat{\Theta}\mathbf{a}_n + \widehat{\mathbf{u}}_n)$. The difference between the two curves represents subject-specific deviations captured by the random effects.

Random-effects regime (df diagnostic). For this example, the random effects operate in a regular (non-saturated) regime. The effective degrees of freedom for the random effects is $\text{df}_U/(NQ) = 0.201$, while the diagnostic cap was set to $\text{df}_U^{\text{max}}/(NQ) = 0.21$. The cap was not activated during optimization, and hence does not constrain the reported solution (Table 1).

Inference for covariate effects. Table 2 reports the estimated covariate effects and their standard errors. p -values are computed using a one-sided test for the boundary null $H_0 : \theta = 0$ versus $H_1 : \theta > 0$ under the non-negativity constraint $\Theta \geq 0$. Both the intercept and the male effect are detected as statistically significant. Moreover, the bootstrap-based standard errors are close to the sandwich-based standard errors, supporting the adequacy of the one-step multiplier (wild) bootstrap approximation in this setting.

Summary. Unlike the LMM, which requires a prescribed time basis, NMF-RE learns the trajectory shape from the data under non-negativity, providing a parsimonious mean-structure summary. This data-driven learning of \widehat{X} constitutes measurement-side variable selection: the non-negative basis automatically identifies which time points contribute to the growth component. On the covariate side, inference on Θ selects the sex effect as significant ($p = 0.001$). The random-effects component is far from saturation, with close SE–BSE agreement (see Appendix G for a detailed comparison with the LMM

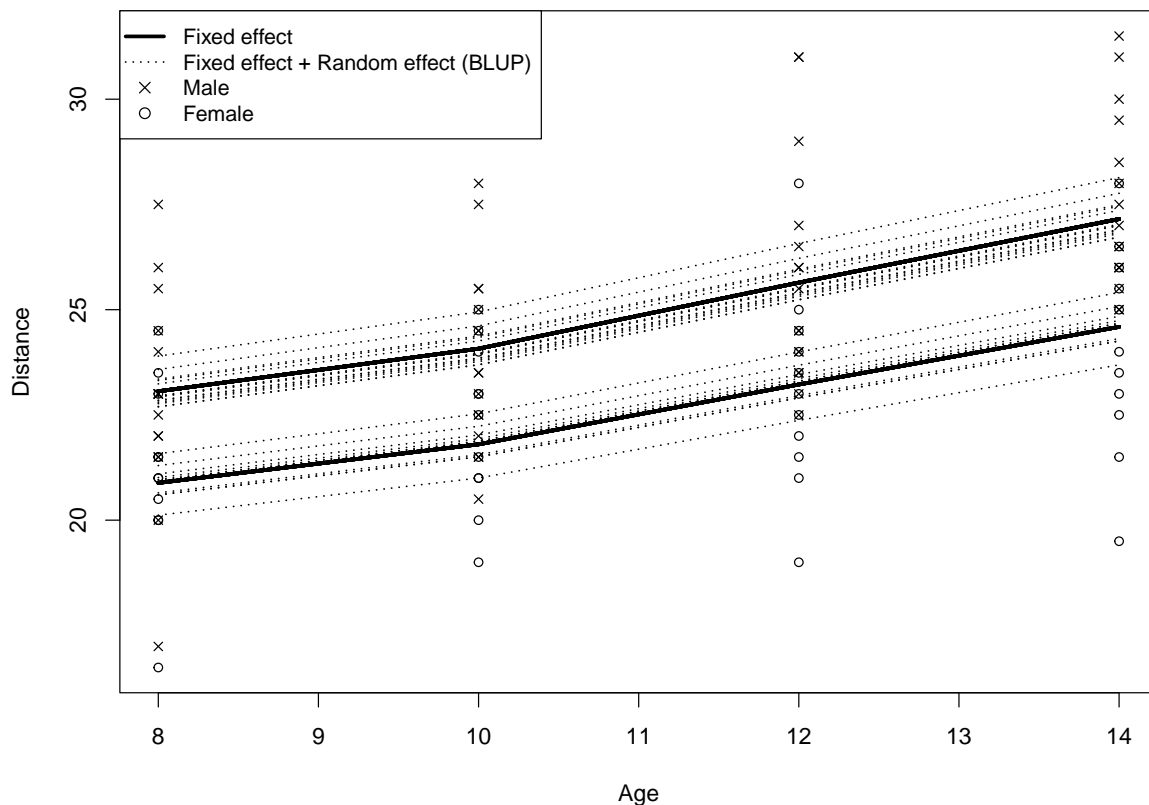


Figure 1

Orthodont growth data ($Q = 1$): observed measurements and fitted curves. Solid lines show fitted values from the fixed-effects component $\widehat{X}\widehat{\Theta}\mathbf{a}_n$, and dashed lines show BLUP-based fits $\widehat{X}(\widehat{\Theta}\mathbf{a}_n + \widehat{\mathbf{u}}_n)$. Points indicate observations (circles: female; crosses: male).

benchmark).

6.2 Holzinger–Swineford cognitive test data

The Holzinger–Swineford (1939) data consist of $P = 9$ cognitive tests for $N = 300$ students (Holzinger & Swineford, 1939; Jöreskog, 1969). The classical confirmatory factor analysis of this dataset posits a three-factor structure (visual, textual, speed); we use NMF-RE to examine whether a comparable structure can be *learned* under non-negativity. As covariates, we use reversed age (`age.rev`), sex (`sex.2`), and school indicator (`school.GW`), all rescaled to $[0, 1]$.

Table 2

Estimated covariate effects for the Orthodont growth data ($Q = 1$). Standard errors are reported from the sandwich estimator (SE) and from the multiplier (wild) bootstrap based on one-step Newton updates (BSE). The Wald statistic is $z = \text{Estimate}/SE$, and p -values are one-sided for $H_0 : \theta = 0$ vs. $H_1 : \theta > 0$ under $\Theta \geq 0$.

Covariate	Estimate	SE	BSE	z	p
Intercept	90.502	2.471	2.450	36.62	< 0.001
Male	9.428	3.056	2.975	3.09	0.0010

NMF-RE specification ($Q = 3$). Motivated by the classical three-factor structure, we set $Q = 3$. The random effects operate in a near-saturated but controlled regime ($\text{df}_U/(NQ) = 0.958$, cap 0.96; Table 1), signaling substantial subject-level heterogeneity beyond the observed covariates. The cap was not activated, so the reported solution is not forced to sit on the boundary.

Learned factor structure (Figure 2). The learned \widehat{X} recovers the familiar three-domain grouping: a component dominated by visual tests (x_1 – x_3), one by textual tests (x_4 – x_6), and one by speed tests (x_7 – x_9), without a prespecified loading pattern (Figure 2). Because \widehat{X} is entrywise non-negative and column-normalized, its entries admit a direct parts-based interpretation as relative test contributions.

Inference for covariate effects (Table 3). Age effects are strongly significant across all three components. Sex and school effects are component-specific: `sex.2` is detected for Factors 2 and 3 but not for Factor 1, while `school.GW` primarily affects Factor 2. SE–BSE agreement holds even under the high saturation ratio.

Supplementary benchmark: confirmatory MIMIC / latent regression in SEM.. As a covariance-based SEM benchmark, we also fitted a confirmatory MIMIC model (Bollen, 1989; Jöreskog & Goldberger, 1975) using `lavaan` (Rosseel, 2012) with the textbook three-factor specification and robust standard errors (see Appendix G for full

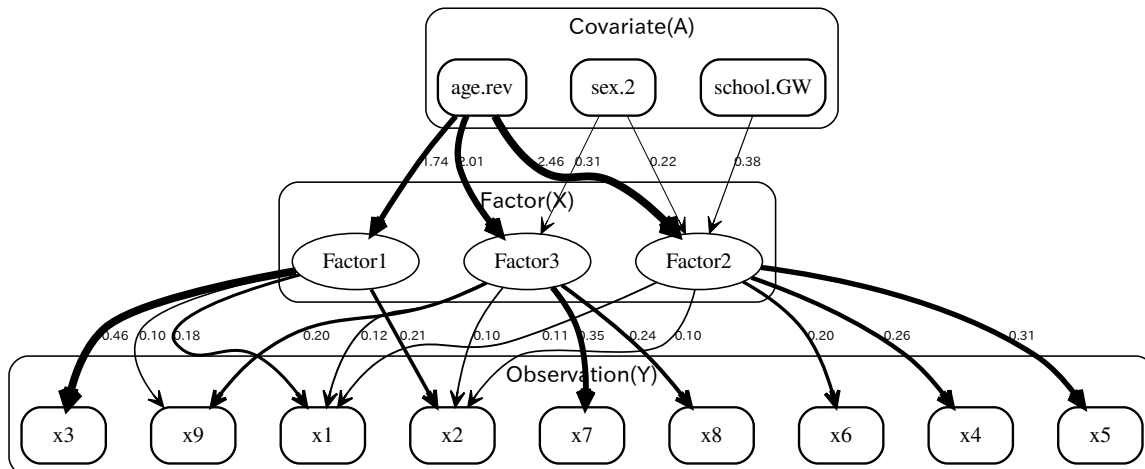


Figure 2

Holzinger–Swineford cognitive test data ($Q = 3$): estimated structure linking observed tests (Y), latent components (X), and covariates (A) under the NMF-RE model.

results). The MIMIC analysis confirms that all three covariates have nontrivial impact on the latent structure under the confirmatory specification. One notable difference is that the MIMIC model detects a significant *negative* sex effect on the visual factor, which the non-negativity constraint $\Theta \geq 0$ in NMF-RE projects to zero; this illustrates that $\Theta \geq 0$ trades the ability to detect sign-unrestricted effects for interpretability and sparsity.

Summary. Unlike confirmatory SEM, NMF-RE learns the measurement structure directly from data under non-negativity, recovering the three-domain grouping without a prespecified loading pattern. This illustrates measurement-side variable selection: the nine tests are partitioned into visual, textual, and speed components by \widehat{X} alone. On the covariate side, inference on Θ performs component-specific covariate selection—age is universally significant, whereas sex and school effects are detected only for specific factors (Table 3). The random-effects regime is near-saturated but non-binding, with close SE–BSE agreement (see Appendix G for a detailed MIMIC comparison).

Table 3

Estimated covariate effects for the Holzinger–Swineford cognitive test data ($Q = 3$) under NMF-RE. Format as in Table 2.

Covariate	Basis	Estimate	SE	BSE	z	p
age.rev	Factor1	1.738	0.089	0.087	19.54	< 0.001
age.rev	Factor2	2.456	0.100	0.100	24.46	< 0.001
age.rev	Factor3	2.015	0.078	0.077	25.74	< 0.001
sex.2	Factor1	0.000	0.059	0.036	0.00	0.5000
sex.2	Factor2	0.220	0.071	0.069	3.10	0.0010
sex.2	Factor3	0.309	0.060	0.059	5.14	< 0.001
school.GW	Factor1	0.000	0.058	0.032	0.00	0.5000
school.GW	Factor2	0.378	0.075	0.075	5.05	< 0.001
school.GW	Factor3	0.000	0.069	0.042	0.00	0.5000

6.3 Origin–destination flow data with hub-based covariates

We consider an origin–destination (OD) flow table from the Japanese National Road Traffic Census (Ministry of Land, Infrastructure, Transport and Tourism, 2021). Let $F \in \mathbb{R}_{\geq 0}^{47 \times 47}$ denote the OD table; we analyze the log-transformed $\log(1 + F_{ij})$. Four metropolitan hubs (Tokyo, Aichi, Osaka, Fukuoka) are selected as covariates ($K = 4$), with destinations as units ($N = 47$). The response matrix $Y \in \mathbb{R}^{43 \times 47}$ collects outbound flows from the remaining $P = 43$ non-hub origins, and $A \in \mathbb{R}^{4 \times 47}$ collects hub outbound flows.

NMF-RE specification ($Q = 4$). With $Q = 4$ matching the number of hubs, the random effects are strongly regularized ($\text{df}_U/(NQ) = 0.013$; Table 1), indicating that most variation is explained by the hub-based mean structure.

Probability-like scores and spatial visualization. Because fitted scores are non-negative, normalizing $\hat{B} = \hat{\Theta}A$ to column sums yields simplex-like representations from which a hard clustering is obtained by $\arg \max_q$. Figure 3 colors each destination by its

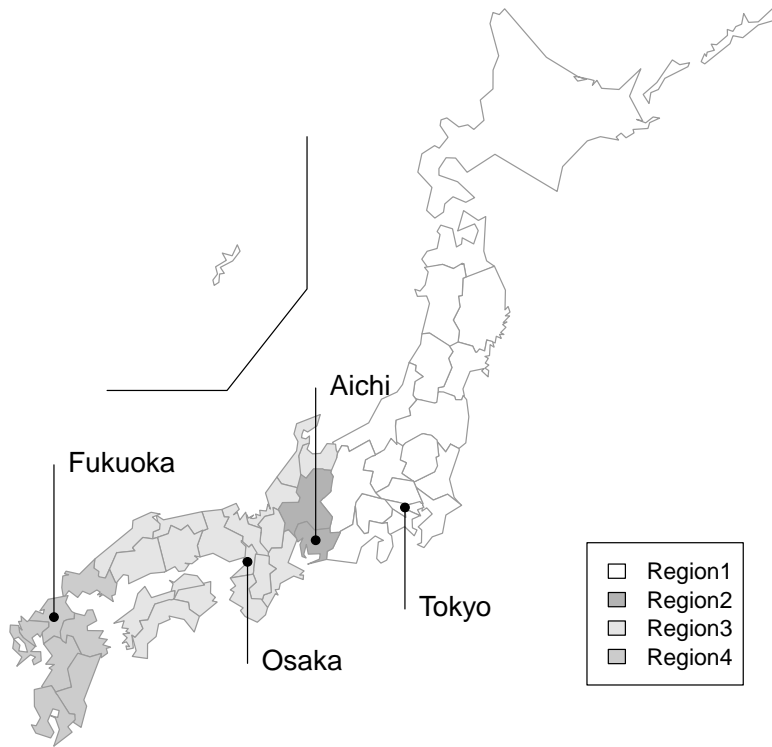


Figure 3

OD-HUB data ($Q = 4$): spatial visualization of the latent components identified by the NMF-RE model. Each destination prefecture is colored according to the dominant latent component based on the fitted latent scores.

dominant component; each component aligns primarily with one hub, yielding a clear geographic partition.

Inference for hub effects (Table 4). $\hat{\Theta}$ exhibits a near one-to-one hub-component association: each component has a single dominant hub coefficient, with cross-loadings at exact zero under $\Theta \geq 0$. SE-BSE agreement holds for the dominant coefficients; boundary coefficients show smaller BSE due to projection onto $\Theta \geq 0$.

Supplementary benchmark: projection pursuit regression (PPR). As a flexible regression benchmark, we also fitted multivariate PPR (Friedman, 1984; Friedman & Stuetzle, 1981) with $M = 4$ ridge terms (see Appendix G for details). The estimated

projection directions mix the four hubs within each term, so interpretability hinges on ridge-function diagnostics rather than a direct hub-to-component correspondence.

Summary. NMF-RE yields a structured parts-based decomposition with non-negative scores that enable probability-like representations and transparent geographic clustering (Figure 3; see Appendix G for a detailed PPR comparison). Measurement-side selection assigns each destination to its dominant hub region via \widehat{X} , while covariate-side selection reveals a sharp one-to-one mapping between origin hubs and regional components (Table 4): each hub covariate loads exclusively on one component, with all off-diagonal effects estimated at zero. The very small saturation ratio implies that the partition is essentially driven by the fixed-effects mean structure; the dfU-cap is triggered transiently but the final solution is non-binding.

6.4 Topic model with historical covariates

As a final illustration, we apply the proposed NMF-RE framework to a text analysis problem based on U.S. presidential inaugural addresses. Following standard preprocessing in R using `quanteda` (Benoit et al., 2018), we represent the corpus as a document–term matrix of non-negative word counts. We retain words that appear at least 100 times across the corpus, yielding a moderate vocabulary size ($P = 67$) over $N = 59$ documents.

Historical covariates (era indicators) and coding. To examine systematic historical shifts in thematic structure, we introduce three mutually exclusive era indicators as covariates: (i) Early (1775–1865; independence to the Civil War), (ii) Industrial (1865–1945; industrialization and overseas expansion), and (iii) Postwar (1945–; post–World War II). These indicators form the rows of A *without an intercept*, so that each document belongs to exactly one era. Under this coding, each column of $\widehat{\Theta}A$ equals the era-specific expected latent-score vector, and the fixed-effects reconstruction $\widehat{X}\widehat{\Theta}A$ induces a step-function (piecewise-constant) pattern across eras when documents are ordered chronologically.

NMF-RE specification and random-effects regime. We fit NMF-RE with latent dimension $Q = 3$, interpreting each column of the fitted basis \widehat{X} as a topic-specific word profile. Let $\widehat{B} = \widehat{\Theta}A$ denote the fixed-effects latent-score matrix. For this dataset, random effects are strongly regularized: the saturation ratio is $\text{df}_U/(NQ) = 0.007$ with diagnostic cap $\text{df}_U^{\text{max}}/(NQ) = 0.02$, and the cap was activated at least once during optimization (Table 1). Thus, most systematic variation is attributed to the fixed-effects mean structure, while remaining within-era idiosyncrasies are heavily shrunk through \widehat{U} .

Learned topics. Each column of \widehat{X} is a topic-specific word profile; words with $\widehat{X}_{pq}/\sum_{q'}\widehat{X}_{pq'} > 0.5$ are taken as representative. The three components are (illustratively): Topic 1 (institutional/legal), Topic 2 (union/constitutional/foreign), and Topic 3 (modern civic rhetoric).

Fixed-effects topic proportions (Figure 4). Normalizing \widehat{B} within each document yields topic proportions $\widehat{\pi}_{qn} = \widehat{B}_{qn}/\sum_{q'}\widehat{B}_{q'n}$. Figure 4 displays these proportions chronologically, highlighting systematic stepwise shifts in topic prevalence across eras.

Inference for era-specific effects (Table 5). With no-intercept coding, each coefficient is an era-specific expected latent-score level. The postwar era is dominated by Topic 3, while Topics 1 and 2 are concentrated in earlier eras, with close SE–BSE agreement.

Supplementary benchmark: structural topic model (STM) with the same era design. As a robustness check, we also fitted a structural topic model (STM) with $Q = 3$ (Roberts et al., 2014, 2019) using the same no-intercept era coding (see Appendix G for full results). After aligning topics by representative words, STM corroborates the same qualitative historical pattern: the civic-rhetoric topic increases sharply from Early to Postwar, whereas the institutional/legal topic becomes small in the Postwar era.

Summary. NMF-RE adds explicit mean-structure inference with non-negative word profiles and complexity diagnostics to the era signal corroborated by STM (see Appendix G for a detailed comparison). Measurement-side selection is visible in \widehat{X} , which

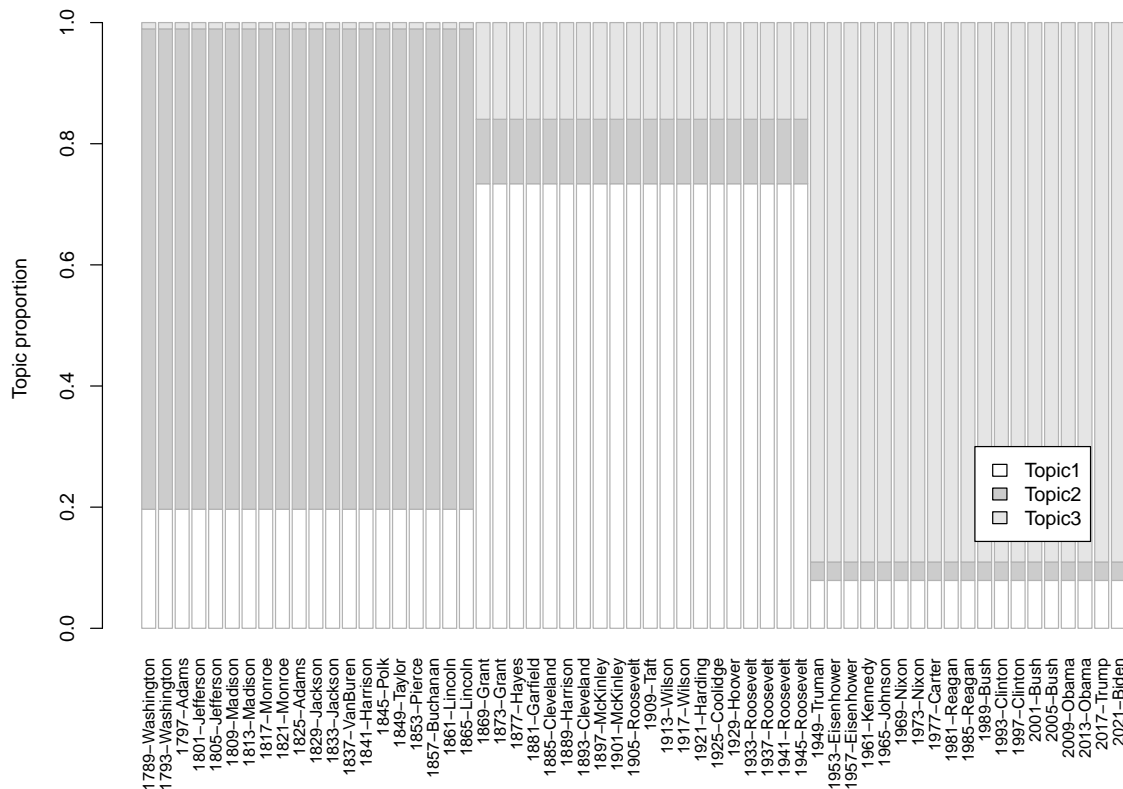


Figure 4

Topic model with historical covariates ($Q = 3$): estimated topic proportions based on the fixed-effects component $\widehat{X}\widehat{\Theta}A$. Each bar corresponds to one inaugural address (document), illustrating systematic shifts in topic prevalence across historical eras.

assigns each word to its dominant topic (institutional/legal, civic-rhetoric, or union/constitutional). Covariate-side selection through Θ reveals that each era is characterized by a distinct dominant topic—Topic 2 (union/constitutional) for the Early era, Topic 1 (institutional/legal) for the Industrial era, and Topic 3 (civic rhetoric) for the Postwar era—with nonsignificant entries identifying the absent era–topic combinations (Table 5). The random-effects component is effectively inactive ($df_U/(NQ)$ near zero), indicating that the temporal pattern is driven by the fixed-effects component.

7 Discussion

This paper proposed NMF-RE, a mean-structure extension of covariate-driven NMF that combines ridge-regularized random effects with one-step multiplier-bootstrap inference for Θ , bridging mixed-effects modeling and non-negative low-rank representations. The four empirical examples illustrated the method across diverse settings: longitudinal growth (Orthodont), cognitive test batteries (Holzinger–Swineford), spatial origin–destination flows (OD–HUB), and presidential address topics. These applications spanned saturation ratios from nearly zero to over 0.95, demonstrating that the dfU-cap and complexity diagnostics remain informative across contrasting random-effects regimes.

7.1 Interpretation and practical diagnostics

A central practical issue in NMF-RE is the potential for near-saturation when the random effects are weakly regularized. The saturation ratio $df_U/(NQ)$ provides a scale-free summary of the operating regime, and the dfU-cap prevents penalty collapse and degenerate inference (Appendix E demonstrates this failure mode in a controlled stress test). For transparent reporting, we recommend presenting $df_U/(NQ)$, the cap ratio, whether the cap was ever activated, and whether the final solution is binding or non-binding.

For inference, close agreement between sandwich-based and bootstrap-based standard errors (SE–BSE agreement) indicates that the one-step linearization is adequate; all four empirical illustrations exhibited such agreement. When discrepancies are large, practitioners should check convergence, increase B , examine dfU-cap status, or reduce model complexity. Near-boundary coefficients should be assessed with directional tests and percentile summaries rather than two-sided Wald approximations (see Appendix D for details).

7.2 Variable selection through non-negative latent structure

As outlined in the Introduction, NMF-RE achieves variable selection on two complementary sides. On the *measurement side*, the non-negativity constraint plays a role

analogous to rotation or sparsity penalties in factor analysis, but induces sparse, parts-based loadings as a structural consequence rather than through an explicit penalty such as the LASSO. All four empirical illustrations confirm this mechanism: \widehat{X} consistently groups observed variables into interpretable components—cognitive test domains, growth trajectories, geographic regions, or word topics—without a prespecified loading pattern.

On the *covariate side*, formal inference on Θ identifies which covariates significantly affect which components, providing a test-based covariate selection. Across the examples, the estimated Θ reveals component-specific patterns in which some covariate effects are strongly significant while others are estimated at exactly zero, yielding a selective structure without an explicit sparsity penalty. Together, these two mechanisms allow NMF-RE to serve as a data-driven variable selection tool in psychometric and related settings, complementing traditional regularization-based approaches with a constraint-driven, interpretable alternative.

7.3 Methodological limitations

The proposed inference is explicitly *conditional* on the estimated regularized solution $(\widehat{X}, \widehat{U})$. Accordingly, it does not attempt to propagate uncertainty due to estimation of X and U . This post-regularization perspective is deliberate: it yields stable and scalable uncertainty quantification for the low-dimensional target Θ while avoiding repeated constrained optimization. At the same time, conditional inference may be conservative or anti-conservative depending on the extent to which variability in $(\widehat{X}, \widehat{U})$ would affect the distribution of $\widehat{\Theta}$ in a given application. Relatedly, NMF models are only partially identifiable up to scaling and permutation, and the non-convex objective can have local minima; in practice, warm starts and multiple initializations may be useful when Q is not small or when the covariate design is highly imbalanced.

The working Gaussian scale model is used to define scores and information matrices, while robustness is pursued through sandwich covariance estimation and multiplier bootstrap resampling of score contributions. These choices are standard in misspecified

likelihood and post-regularization settings; nevertheless, establishing formal validity under general non-Gaussian data generating processes and under data-adaptive selection of $(\widehat{X}, \widehat{U})$ remains an important direction for further theoretical work. Finally, the non-negativity constraint $\Theta \geq 0$ can induce truncation and skewness for near-boundary coefficients, motivating the boundary-aware diagnostics discussed in Section 7.1.

7.4 Extensions and future work

Several extensions are natural. First, developing selection-aware inference that propagates uncertainty from $(\widehat{X}, \widehat{U})$ into Θ would clarify when conditional inference is adequate; however, resampling X is complicated by non-convexity and label switching. Second, replacing the squared-loss criterion by count-data likelihoods (e.g., Poisson) would extend NMF-RE to settings with strongly mean-dependent variance. Third, boundary-aware interval constructions beyond normal approximations are needed for principled summaries when many coefficients are near zero. Fourth, data-driven selection of the rank Q is an open problem shared with all low-rank models; integrating information-criterion or cross-validation methods into the NMF-RE framework would reduce reliance on external rank diagnostics.

7.5 Concluding remarks

NMF-RE provides a practical bridge between classical mixed-effects ideas and modern non-negative low-rank representations, supporting a mean-structure-centric strategy for inference in constraint-based latent-variable models with explicit complexity control and implicit variable selection. The empirical illustrations showed that benchmark-specific methods (LMM, factor analysis, STM) can corroborate NMF-RE findings within their own domains, while NMF-RE offers a unified framework that accommodates all four settings under a single model and inference apparatus.

Statements and Declarations

Funding. This work was partly supported by JSPS KAKENHI Grant Numbers 22K11930, 25K15229, 24K03007, 25H00482, the project research fund by the Research Center for

Sustainability and Environment at Shiga University, and a research grant from the Fuji Seal Foundation.

Competing Interests. The author has no relevant financial or non-financial interests to disclose.

Ethical Approval. Not applicable.

Data Availability. All empirical data sets used are publicly available through R packages (`nlme`, `lavaan`, `quanteda`) or the Japanese e-Stat portal (<https://www.e-stat.go.jp>). All analysis scripts, simulation code, and pre-processed data files needed to reproduce the results in this paper are available at <https://github.com/ksatohds/nmfre-paper>.

Code Availability. The R package `nmfkc` implementing the covariate-driven NMF used for initialization is publicly available at <https://ksatohds.github.io/nmfkc/>.

Use of AI Tools. Claude Code (Anthropic, Claude Opus 4 model, <https://claude.ai/code>, accessed February–March 2026) was used for \LaTeX formatting, compilation, cross-reference verification, and manuscript proofreading. No scientific content—including the methodology, mathematical derivations, data analysis, or interpretation of results—was generated by AI tools. The author assumes full responsibility for the accuracy and integrity of all content.

Table 4

Estimated covariate effects for the OD-HUB data ($Q = 4$). Format as in Table 2.

Covariate	Basis	Estimate	SE	BSE	z	p
Tokyo	Region1	8.896	0.801	0.763	11.11	< 0.001
Tokyo	Region2	0.000	0.302	0.165	0.00	0.5000
Tokyo	Region3	0.000	0.292	0.163	0.00	0.5000
Tokyo	Region4	0.000	0.250	0.153	0.00	0.5000
Aichi	Region1	0.000	0.597	0.354	0.00	0.5000
Aichi	Region2	4.381	0.633	0.642	6.92	< 0.001
Aichi	Region3	0.000	0.524	0.309	0.00	0.5000
Aichi	Region4	0.000	0.503	0.265	0.00	0.5000
Osaka	Region1	0.000	0.546	0.295	0.00	0.5000
Osaka	Region2	0.000	0.322	0.197	0.00	0.5000
Osaka	Region3	6.895	0.637	0.656	10.82	< 0.001
Osaka	Region4	0.000	0.413	0.230	0.00	0.5000
Fukuoka	Region1	0.000	0.483	0.200	0.00	0.5000
Fukuoka	Region2	0.000	0.190	0.095	0.00	0.5000
Fukuoka	Region3	0.000	0.520	0.254	0.00	0.5000
Fukuoka	Region4	5.575	0.373	0.374	14.94	< 0.001

Table 5

Estimated covariate effects for the topic model ($Q = 3$). Format as in Table 2.

Period	Topic	Estimate	SE	BSE	z	p
Early (1775–1865)	Topic 1	46.744	12.036	11.914	3.88	< 0.001
Early (1775–1865)	Topic 2	188.558	36.392	37.162	5.18	< 0.001
Early (1775–1865)	Topic 3	2.491	4.647	3.362	0.54	0.2960
Industrial (1865–1945)	Topic 1	164.855	24.441	24.985	6.75	< 0.001
Industrial (1865–1945)	Topic 2	23.901	13.113	12.944	1.82	0.0342
Industrial (1865–1945)	Topic 3	35.862	14.349	14.026	2.50	0.0062
Postwar (1945–)	Topic 1	16.528	9.538	8.952	1.73	0.0416
Postwar (1945–)	Topic 2	6.361	7.375	5.826	0.86	0.1942
Postwar (1945–)	Topic 3	186.287	11.182	10.846	16.66	< 0.001

Appendix A

Practical Calibration of the dfU-Cap

Let $r^{\max} \equiv \text{df}_U^{\max}/(NQ)$ denote the cap ratio and let X_{fix} be the basis obtained from the covariate-driven NMF fit with $U \equiv 0$ used for initialization. For a fixed X , define the saturation-ratio function

$$r_X(\lambda) \equiv \frac{\text{df}_U(\lambda)}{NQ} = \frac{1}{Q} \sum_{q=1}^Q \frac{d_q}{d_q + \lambda},$$

where d_1, \dots, d_Q are the eigenvalues of $X^\top X$. Computing $r_{X_{\text{fix}}}(\lambda)$ over a log-scale grid yields a simple “ $\lambda \leftrightarrow r$ ” lookup before running the full NMF-RE algorithm. If values $\lambda < \lambda_{\min}$ are deemed implausible for the application, then setting

$$\text{df}_U^{\max} = r_{X_{\text{fix}}}(\lambda_{\min}) NQ$$

provides a principled cap that avoids trial-and-error scans. This pre-calibration uses X_{fix} only to choose df_U^{\max} ; the cap is enforced during optimization using the current X through $\lambda_{\text{cap}}(X)$.

For transparent reporting, we distinguish (i) whether the cap was ever activated during optimization and (ii) whether the final converged solution is *binding* ($\text{df}_U = \text{df}_U^{\max}$) or *non-binding* ($\text{df}_U < \text{df}_U^{\max}$). We report the realized saturation ratio $\text{df}_U/(NQ)$, the cap ratio $\text{df}_U^{\max}/(NQ)$, the final $\hat{\lambda}$, and the activation/binding indicators.

Appendix B

Estimation Algorithm

Algorithm 1 presents the complete block-wise estimation procedure for NMF-RE with a df-based cap for random effects, as described in Section 3 of the main text.

Remark (stabilized multiplicative updates and objective monitoring).

When U is real-valued, the intermediate matrices $B_U = \Theta A + U$ and $Y_U = Y - XU$ can contain negative entries, so the classical Euclidean multiplicative updates are not directly applicable. We therefore use elementwise positive parts $B_U^+ = \max(B_U, 0)$ and $Y_U^+ = \max(Y_U, 0)$ only as stabilized surrogates to keep multiplicative ratios well-defined and to preserve non-negativity of X and Θ . Because these stabilized updates are not derived as an exact majorization–minimization scheme for the full objective $\mathcal{L}(X, \Theta, U)$, we explicitly monitor \mathcal{L} after each block update and employ a simple descent safeguard (rollback or damping) if an iteration increases the objective. In our numerical experiments, this safeguard was rarely activated, but it provides a transparent guarantee against pathological steps.

Remark (warm-start variance estimation). Algorithm 1 treats $\lambda > 0$ as a given initial penalty, adjusted only upward by the dfU cap. In practice, $\lambda = \sigma^2/\tau^2$ depends on the noise variance σ^2 , which is unknown before fitting. Our implementation therefore uses a warm-start schedule: σ^2 is held at a fixed initial value (e.g., $\sigma^2 = 1$) for the first several dozen iterations while the block-wise updates stabilize (X, Θ, U) , and is then gradually updated toward the current residual mean square $\|Y - X(\Theta A + U)\|_F^2/(PN)$ via an exponential moving average with a small learning rate. Because the dfU cap provides a floor on λ , this adaptive schedule cannot drive λ to zero; it merely aligns the working variance scale with the data without destabilizing the optimization.

Algorithm 1 Block-wise estimation of NMF-RE with a df-based cap for random effects

Require: Non-negative data $Y \in \mathbb{R}_{\geq 0}^{P \times N}$, covariates $A \in \mathbb{R}^{K \times N}$, rank Q , initial penalty

$\lambda > 0$, cap level df_U^{\max} , tolerance `tol`, maximum iterations `maxit`.

Ensure: $\widehat{X}, \widehat{\Theta}, \widehat{U}$ and final λ .

Initialize:

1: Fit covariate-driven NMF with $U \equiv 0$ to get (X, Θ) ; set $U \leftarrow 0$.

2: Normalize X so that $\mathbf{1}_P^\top X = \mathbf{1}_Q^\top$ and absorb scaling into Θ .

3: **for** $t = 1, 2, \dots, \text{maxit}$ **do**

4: Compute current objective $L_{\text{old}} \leftarrow \|Y - X(\Theta A + U)\|_F^2 + \lambda \|U\|_F^2$.

(i) Enforce df cap (diagnostic safeguard):

5: Compute eigenvalues d_1, \dots, d_Q of $X^\top X$.

6: Find $\lambda_{\text{cap}}(X) = \inf\{\lambda' > 0 : N \sum_{q=1}^Q \frac{d_q}{d_q + \lambda'} \leq \text{df}_U^{\max}\}$ (e.g., bisection).

7: $\lambda \leftarrow \max\{\lambda, \lambda_{\text{cap}}(X)\}$.

(ii) U -step (ridge / BLUP-like update):

8: $M \leftarrow (X^\top X + \lambda I_Q)^{-1} X^\top$.

9: $U \leftarrow M(Y - X(\Theta A))$.

10: Row-center U so that each row has mean zero across units.

(iii) X -step (stabilized multiplicative update + renormalization):

11: $B_U \leftarrow \Theta A + U$, $B_U^\dagger \leftarrow \max(B_U, 0)$ (elementwise).

12: $X_{\text{cand}} \leftarrow X \odot \left(Y (B_U^\dagger)^\top \right) \oslash \left(X (B_U^\dagger (B_U^\dagger)^\top) \right)$.

13: Normalize columns: $X_{\text{cand}} \leftarrow X_{\text{cand}} D^{-1}$ so that $\mathbf{1}_P^\top X_{\text{cand}} = \mathbf{1}_Q^\top$.

14: Rescale $(\Theta, U) \leftarrow (D\Theta, DU)$ to keep $X(\Theta A + U)$ unchanged.

(iv) Θ -step (stabilized multiplicative update):

15: $Y_U \leftarrow Y - XU$, $Y_U^\dagger \leftarrow \max(Y_U, 0)$ (elementwise).

16: $\Theta_{\text{cand}} \leftarrow \Theta \odot \left(X^\top Y_U^\dagger A^\top \right) \oslash \left((X^\top X \Theta) (A A^\top) \right)$.

(v) Descent safeguard using the true working objective:

17: Form candidate $(X, \Theta) \leftarrow (X_{\text{cand}}, \Theta_{\text{cand}})$ and compute $L_{\text{new}} \leftarrow \|Y - X(\Theta A + U)\|_F^2 + \lambda \|U\|_F^2$.

18: **if** $L_{\text{new}} > L_{\text{old}}$ **then**

19: (Optional) apply damping / rollback, e.g., set $X \leftarrow X_{\text{old}}, \Theta \leftarrow \Theta_{\text{old}}$ and skip the

Appendix C

Asymptotic Justification of the One-Step Map

Conditional on (\widehat{X}, λ) and with U profiled out by ridge regression, $\widehat{\Theta}$ can be viewed as a (possibly misspecified) Z-estimator solving $\sum_{n=1}^N \text{vec}\{S_n(\Theta)\} = \mathbf{0}$. Under standard regularity conditions for Z-estimators—smoothness of the score map, nonsingularity of the Jacobian (equivalently, the reduced information) at the target, and an initial estimator $\widetilde{\Theta}$ that is \sqrt{N} -consistent and lies in an $O_p(N^{-1/2})$ neighborhood of the target—a one-step Newton update

$$\text{vec}(\Theta^{\text{os}}) = \text{vec}(\widetilde{\Theta}) - \mathcal{I}(\widetilde{\Theta})^{-1} \sum_{n=1}^N \text{vec}\{S_n(\widetilde{\Theta})\}$$

is asymptotically equivalent to the fully iterated Z-estimator (the root of the estimating equation) in the interior regime, in the sense that $\sqrt{N}(\Theta^{\text{os}} - \widehat{\Theta}) \rightarrow 0$ in probability. This is a classical consequence of asymptotic linearity for M/Z-estimators and underlies one-step/debiased constructions in post-regularization inference (see, e.g., Huber et al., 1967; Javanmard & Montanari, 2014; Taylor & Tibshirani, 2015; van de Geer et al., 2014; White, 1980). In our bootstrap construction, $S^*(\widehat{\Theta})$ in the one-step formula denotes the multiplier-resampled score (Sections 4.4–4.5 of the main text). The non-negativity constraint $\Theta \geq 0$ is handled by projection of one-step replicates; near the boundary, the limiting distribution can be non-Gaussian, so directional tests and percentile-type summaries are more appropriate than symmetric Wald approximations.

Appendix D

Validity, Scope, and Practical Diagnostics

This appendix provides the full discussion of the inferential scope, regularity conditions, and practical diagnostics summarized in Section 4.7 of the main text.

Scope of inference (conditional target). Inference in this paper targets the covariate-effect matrix Θ *conditional on* the selected regularized representation $(\widehat{X}, \widehat{U})$ and the final ridge level λ produced by the estimation algorithm. Accordingly, sampling variability is assessed through unit-wise (column-wise) score contributions given fixed covariates A , while additional uncertainty due to the non-convex estimation of X and the regularized fit of U is treated as part of the post-regularization approximation (Javanmard & Montanari, 2014; van de Geer et al., 2014; White, 1980).

Estimating-equation viewpoint and robust covariance. With (\widehat{X}, λ) treated as fixed and U profiled out by ridge regression, $\widehat{\Theta}$ can be viewed as a (possibly misspecified) Z-estimator solving the estimating equation

$$\sum_{n=1}^N \text{vec}\{S_n(\Theta)\} = \mathbf{0},$$

where $S_n(\Theta)$ is the unit-wise score contribution. Under standard regularity conditions for M/Z-estimators—notably, (i) independence across units n (or validity of a cluster-robust adaptation), (ii) finite second moments of the score contributions, and (iii) nonsingularity of the reduced information matrix—the sandwich covariance estimator provides large-sample robust standard errors even under a misspecified Gaussian working model (Cameron et al., 2008; Huber et al., 1967; White, 1980).

Multiplier (wild) bootstrap as a fast resampling approximation. The multiplier (wild) bootstrap resamples the empirical distribution of the score contributions by random reweighting, avoiding repeated constrained re-optimization. Under mild moment conditions, such multiplier schemes consistently approximate the distribution of smooth functionals of estimating-equation solutions (Cameron et al., 2008; Mammen, 1993). Combined with the one-step Newton map, this yields a computationally efficient

approximation to resampling-based uncertainty quantification in our post-regularization setting (Javanmard & Montanari, 2014; van de Geer et al., 2014).

Boundary behavior under $\Theta \geq 0$. Because the one-step update is unconstrained, bootstrap replicates are projected onto the non-negative orthant. Coefficients near the boundary can therefore exhibit truncation and skewness, so directional (one-sided) tests and percentile-type bootstrap summaries are often more appropriate than symmetric Gaussian Wald approximations. In such boundary regimes, discrepancies between sandwich-based standard errors and bootstrap-based standard errors can arise mechanically from projection and should not be interpreted as a failure of the one-step linearization.

Practical diagnostics and reporting. For transparent reporting and to guard against near-saturated random-effects updates, we recommend documenting: (i) the saturation ratio $df_U/(NQ)$ and the cap level $df_U^{\max}/(NQ)$ (and, when relevant, an upper-tail summary such as $dfU_{0.99}$ over iterations or across restarts); (ii) whether the dfU-cap was ever activated during optimization and whether the final solution is binding ($df_U = df_U^{\max}$) or non-binding ($df_U < df_U^{\max}$), together with the final $\hat{\lambda}$; (iii) agreement between sandwich-based and bootstrap-based standard errors for coefficients well inside the feasible region; and (iv) sensitivity to initialization (multiple starts) and convergence behavior when Q is moderate or large. These checks help assess whether the selected low-rank representation is sufficiently stable for the intended conditional inference on Θ .

Appendix E

Stress Test for Random-Effects Saturation

This appendix reports an additional targeted stress experiment designed to verify that the dfU-cap functions as a safety device against random-effects saturation. The stress test uses a more flexible setting ($P = 4$, $Q = 3$, $N = 100$) than the baseline simulation in the main text, where the working random-effects penalty is intentionally weakened. *This experiment is designed as a failure-mode demonstration (near-saturation and $\hat{\lambda}$ collapse), not as a benchmark of inferential accuracy under well-regularized fits.* Specifically, we initialize the variance ratio so that $\lambda = \sigma^2/\tau^2$ is extremely small by using $\sigma_{\text{fit}}^2 = 1$ and $\tau_{\text{fit}}^2 = 1000$, which (without safeguards) promotes a near-saturated U update and can drive $\hat{\lambda}$ toward zero.

For this stress test we use a synthetic three-trend basis matrix $X_{\text{true}} \in \mathbb{R}^{4 \times 3}$ with column sums normalized to one:

$$X_{\text{true}} = \left((0.45, 0.30, 0.15, 0.10)^\top, (0.25, 0.25, 0.25, 0.25)^\top, (0.10, 0.15, 0.30, 0.45)^\top \right), \quad \mathbf{1}_P^\top X_{\text{true}} = \mathbf{1}_3^\top.$$

The intercept is split evenly across the three trends, and the male effect is placed on Trend1 only: $\Theta_{\text{true}}[\text{Trend1, male}] = 9.4285$ and $\Theta_{\text{true}}[\text{Trend2, male}] = \Theta_{\text{true}}[\text{Trend3, male}] = 0$, while $\Theta_{\text{true}}[\text{Trend}q, \text{intercept}] = 90.502/3$ for $q = 1, 2, 3$. The data are generated from the same data-generating process as the baseline simulation with $U \in \mathbb{R}^{3 \times N}$.

We compare three dfU-cap settings: a strict cap $\text{dfU}^{\text{max}}/(NQ) = 0.21$, a loose cap 0.99, and no cap. The goal is to demonstrate what happens when U becomes (nearly) saturated and whether dfU-cap prevents the resulting degeneracy in inference for Θ .

Failure mode without dfU-cap. Table E1 is a targeted failure-mode demonstration of random-effects saturation. With the strict cap (0.21), $\text{dfU}_{0.99}$ stays near 0.21 and the fitted penalty remains in a stable regime (MeanLambda around 1.3–1.7), keeping the U -update away from near-saturation. In this regime, the BSE-based one-sided size under the Null remains close to 5% and Wald coverage is near (or slightly above) nominal.

When the cap is loose (0.99) or turned off, $\text{dfU}_{0.99}$ approaches one and the fitted

penalty collapses (MeanLambda below 10^{-3}), corresponding to an almost unpenalized U update. Under the Null this produces *degenerate* inference: the Wald test essentially never rejects and coverage inflates to 1.00, indicating that U absorbs nearly all idiosyncratic variation and leaves little stable information for Θ .

Under the Alternative, rejection remains high across caps, but coverage is poor in all three settings. Notably, coverage under the strict cap (0.250/0.280) is *lower* than under the loose cap (0.650/0.640), because the strict cap constrains U more heavily and thereby redirects additional bias into $\hat{\Theta}$. This is expected in the present stress design: the intentionally weak initial penalty combined with a higher-dimensional random-effects space ($Q = 3$) creates a regime in which $\hat{\theta}$ is substantially biased under all cap settings, so coverage alone is not the appropriate success criterion here. What the table *does* demonstrate is the contrast between the strict cap and the loose/off settings: without the cap, the fitted penalty collapses ($\hat{\lambda} \approx 0$) and inference becomes degenerate, whereas the strict cap keeps $\hat{\lambda}$ in a stable regime and preserves meaningful (albeit imperfect) uncertainty quantification. Under well-calibrated conditions—as in the baseline $Q = 1$ simulation (Table F1)—both size and coverage are near nominal. Overall, the stress test shows that dfU-cap is a practically important safeguard: it prevents $\hat{\lambda}$ collapse and blocks pathological inference in regimes that would otherwise admit near-saturated U .

Random-effects complexity monitoring. In the baseline $Q = 1$ design reported in Table F1, the mean saturation ratio $\text{df}_U/(NQ)$ stays near 0.20 under the default cap $\text{df}_U^{\text{max}}/(NQ) = 0.21$, indicating that U is kept in a moderately regularized regime. The $Q = 3$ stress experiment in Table E1 shows why this monitoring matters: if $\text{df}_U/(NQ)$ is allowed to approach one (loose/off cap), the fitted penalty can collapse and inference for Θ can become degenerate or severely distorted.

Table E1

Stress test for random-effects saturation ($P = 4$, $Q = 3$, $N = 100$; $R = 1000$; $B = 1000$).
The fitting routine is initialized with an intentionally weak random-effects penalty ($\sigma_{fit}^2 = 1$, $\tau_{fit}^2 = 1000$), which (without safeguards) encourages $\hat{\lambda}$ to approach zero and U to become nearly saturated. Hypothesis indicates the true-parameter regime: Null ($\theta_{male} = 0$) or Alternative ($\theta_{male} \neq 0$). $dfU_{0.99}$ is the 99th percentile (over Monte Carlo runs) of the saturation ratio $df_U/(NQ)$, and MeanLambda is the Monte Carlo mean of the fitted penalty $\hat{\lambda}$. Reject is the BSE-based Wald rejection rate (one-sided for Null, two-sided for Alternative); Cover is the nominal 95% Wald coverage. This table is intended to demonstrate the degeneracy induced by near-saturation and the protective role of dfU-cap, rather than to provide a general performance comparison across caps.

Hypothesis	r^{\max}	Error	Bias	SD	$dfU_{0.99}$	MeanLambda	Reject	Cover
Null	0.21	Gaussian	0.131	0.220	0.210	1.5988	0.050	0.970
Null	0.99	Gaussian	0.093	0.106	0.990	<0.001	0.000	1.000
Null	off	Gaussian	0.095	0.115	0.999	<0.001	0.000	1.000
Null	0.21	Exp-centered	0.105	0.209	0.210	1.6462	0.020	0.990
Null	0.99	Exp-centered	0.089	0.102	0.990	<0.001	0.000	1.000
Null	off	Exp-centered	0.090	0.104	0.999	<0.001	0.000	1.000
Alternative	0.21	Gaussian	-2.477	1.002	0.210	1.3792	0.960	0.250
Alternative	0.99	Gaussian	-1.151	0.998	0.990	<0.001	1.000	0.650
Alternative	off	Gaussian	-1.710	0.785	0.999	<0.001	1.000	0.110
Alternative	0.21	Exp-centered	-2.388	1.052	0.210	1.3345	0.980	0.280
Alternative	0.99	Exp-centered	-1.118	0.797	0.990	<0.001	1.000	0.640
Alternative	off	Exp-centered	-1.722	0.739	0.999	<0.001	1.000	0.100

Appendix F

Detailed Simulation Results Discussion

This appendix presents the full Monte Carlo results and provides a detailed interpretation.

What SE–BSE agreement does (and does not) validate. When coefficients lie in the interior of the feasible region, agreement between SE and BSE provides direct evidence that the estimator is well captured by its local linearization, which is precisely the approximation used by the one-step multiplier bootstrap. However, in boundary regimes induced by $\Theta \geq 0$, SE–BSE agreement is not the appropriate success criterion: projection of one-step replicates to $\Theta \geq 0$ alters the finite-sample distribution by adding truncation at zero. In that regime, the relevant validation is whether directional testing and interval summaries retain reasonable size and coverage.

Interior regime (Alternative): local linearization works well. Under the Alternative, $\text{Mean}(\text{SE})$ and $\text{Mean}(\text{BSE})$ are close for both error distributions and all N , and coverages approach nominal levels as N increases. This behavior is consistent with the intended post-regularization interpretation: once the selected low-rank structure is stable and coefficients are away from the boundary, the one-step bootstrap provides an accurate local uncertainty approximation.

Boundary regime (Null): projection induces systematic SE–BSE differences. Under the Null, $\text{Mean}(\text{BSE})$ is systematically smaller than $\text{Mean}(\text{SE})$. This is expected: the one-step bootstrap replicates are projected onto $\Theta \geq 0$, which concentrates mass at zero and reduces the empirical spread compared to a symmetric Gaussian Wald approximation. Despite this boundary-induced truncation and the resulting positive bias in $\hat{\theta}_{\text{male}}$, the one-sided rejection rates remain close to the nominal 5% level and Wald-type coverages are slightly conservative across N . Percentile bootstrap intervals show similar coverages, indicating that the projected one-step bootstrap remains practically usable as a boundary-aware uncertainty summary in this setting.

Robustness to skewed observation noise. Replacing Gaussian errors by centered exponential errors yields qualitatively similar bias, SD, RMSE, and coverage patterns. Under the Null, the BSE-based one-sided test becomes mildly more liberal in finite samples, but the deviation is modest and does not worsen with increasing N . Overall, this suggests that the proposed post-regularization inference retains useful stability under moderate deviations from Gaussianity of the measurement noise, at least in this Orthodont-like low-rank design.

Table F1

Monte Carlo results for the male effect θ_{male} under the Orthodont-based design ($P = 4$, $Q = 1$), with $R = 1000$ replicates and multiplier bootstrap size $B = 1000$. Hypothesis indicates the true-parameter regime: Null ($\theta_{male} = 0$) or Alternative ($\theta_{male} \neq 0$). Reject is the Wald rejection rate (one-sided for Null, two-sided for Alternative). Mean is the Monte Carlo average of the standard error estimate (SE or BSE). Entries of the form “a/b” report “SE-based / BSE-based” quantities. PctCover is the coverage of the 95% percentile bootstrap CI, and dfU is the Monte Carlo mean of $df_U/(NQ)$.

N	Hypothesis	Bias	SD	RMSE	Mean	Reject	Cover	PctCover	dfU
<i>Gaussian errors</i>									
27	Null	0.373	0.526	0.645	0.853/0.572	0.064/0.082	0.956/0.951	0.956	0.203
27	Alternative	-0.013	0.919	0.919	0.842/0.826	1.000/1.000	0.912/0.902	0.910	0.201
100	Null	0.179	0.246	0.304	0.443/0.304	0.048/0.055	0.977/0.970	0.978	0.204
100	Alternative	-0.010	0.430	0.430	0.442/0.439	1.000/1.000	0.953/0.952	0.952	0.201
200	Null	0.144	0.185	0.235	0.324/0.226	0.057/0.062	0.970/0.966	0.970	0.206
200	Alternative	-0.011	0.325	0.325	0.324/0.323	1.000/1.000	0.949/0.948	0.946	0.201
<i>Centered exponential errors</i>									
27	Null	0.333	0.473	0.579	0.860/0.567	0.057/0.076	0.969/0.963	0.967	0.201
27	Alternative	-0.025	0.854	0.854	0.850/0.835	1.000/1.000	0.931/0.926	0.928	0.201
100	Null	0.186	0.267	0.326	0.444/0.304	0.063/0.074	0.967/0.963	0.966	0.202
100	Alternative	-0.011	0.457	0.457	0.443/0.441	1.000/1.000	0.939/0.937	0.938	0.201
200	Null	0.155	0.191	0.246	0.323/0.227	0.059/0.071	0.966/0.961	0.964	0.204
200	Alternative	0.009	0.328	0.328	0.323/0.322	1.000/1.000	0.940/0.941	0.938	0.201

Appendix G

Supplementary Benchmark Comparisons

This appendix collects benchmark comparisons with established methods for each of the four empirical illustrations in the main text. These comparisons contextualize the NMF-RE results relative to standard approaches and are not intended as head-to-head performance evaluations.

Orthodont: Linear mixed-effects modeling (LMM)

A standard linear mixed-effects model (LMM) for the Orthodont data specifies a *prescribed* time basis (typically an intercept and a linear age term) and then introduces random effects on that basis. For subject n at age $t \in \{8, 10, 12, 14\}$, a common specification is

$$y_{nt} = (\beta_0 + \beta_{\text{sex:male}_n}) + (\beta_1 + \beta_{\text{age:sex:male}_n})t + (b_{0n} + b_{1n}t) + \varepsilon_{nt},$$

so the analyst must choose and justify a time design *a priori* (and add curvature terms such as t^2 or splines if needed). With only four observation times, this design choice can be consequential.

To make the sex main effect interpretable within the observed age range, we also fit the centered-age form with $t_c = t - 11$:

$$y_{nt} = \beta_0 + \beta_1 t_c + \beta_2 \text{male}_n + \beta_3 t_c \text{male}_n + (b_{0n} + b_{1n} t_c) + \varepsilon_{nt}.$$

In this parameterization, β_2 represents the male effect on distance at age 11. The fitted model indicates that males have a higher mean distance by about 2.32 mm ($\hat{\beta}_2 = 2.321$, $p = 0.0054$), and that the growth rate is also larger for males through the age-by-sex interaction ($\hat{\beta}_3 = 0.305$, $p = 0.0264$), yielding slopes of 0.784 (males) and 0.480 (females) mm/year. Random-effect estimates suggest non-negligible between-subject heterogeneity in both level and slope (SDs about 1.83 and 0.18, respectively) with residual SD about 1.31. The LMM here serves as an orientation benchmark confirming that the Orthodont data exhibit both substantial subject-level heterogeneity and sex-dependent mean structure.

Holzinger–Swineford: Confirmatory MIMIC / latent regression in SEM

To benchmark the NMF-RE mean-structure approach against a classical covariance-based SEM formulation, we fitted a confirmatory MIMIC (multiple indicators multiple causes) model (Bollen, 1989; Jöreskog & Goldberger, 1975) using the `lavaan` package (Rosseel, 2012). Following the textbook three-factor specification, the nine tests were assigned to `visual` (x_1 – x_3), `textual` (x_4 – x_6), and `speed` (x_7 – x_9), and these three factors were regressed on the covariates. We used robust (sandwich) standard errors (MLR) and fixed factor variances to one (`std.lv=TRUE`) to stabilize interpretation of the regression coefficients.

Table G1 reports the latent regression coefficients. In this confirmatory analysis, `sex.2` is significantly associated with the `visual` factor, while `school.GW` is strongly associated with the `textual` factor; `age.rev` shows factor-specific effects, including a clear association with `speed`. Joint Wald tests that constrain each covariate’s three regression coefficients to zero simultaneously reject for `age.rev`, `sex.2`, and `school.GW`, indicating that all three covariates have nontrivial impact on the latent structure under the confirmatory specification. As an overall reference, the fitted MIMIC model yields CFI=0.893, TLI=0.840, RMSEA=0.092, and SRMR=0.061.

OD–HUB: Projection pursuit regression (PPR)

As a flexible regression benchmark that does not impose a low-rank factorization, we also fitted multivariate projection pursuit regression (PPR) (Friedman, 1984; Friedman & Stuetzle, 1981). Treating destinations as observations, we regress the 43-dimensional response $\mathbf{y}_n \in \mathbb{R}^{43}$ on the 4-dimensional hub-flow predictor $\mathbf{a}_n \in \mathbb{R}^4$ using $M = 4$ ridge terms:

$$\mathbf{y}_n = \sum_{m=1}^M \beta_m g_m(\boldsymbol{\alpha}_m^\top \mathbf{a}_n) + \boldsymbol{\varepsilon}_n,$$

where $\boldsymbol{\alpha}_m \in \mathbb{R}^4$ are projection directions shared across responses, $g_m(\cdot)$ are smooth univariate ridge functions, and $\beta_m \in \mathbb{R}^{43}$ are response-specific weights. Using `ppr` in R with $M = 4$ terms (allowing up to 10 candidate terms internally), the fitted model achieved a

Table G1

Confirmatory MIMIC / latent regression results (SEM) for the Holzinger–Swineford data: regression of three textbook factors on covariates. Standard errors are robust (sandwich) under MLR. P-values are two-sided.

Covariate	Factor	Estimate	SE	z	p
age.rev	visual	0.075	0.075	0.998	0.318
age.rev	textual	0.183	0.059	3.131	0.002
age.rev	speed	-0.264	0.073	-3.605	< 0.001
sex.2	visual	-0.427	0.162	-2.642	0.008
sex.2	textual	0.119	0.128	0.934	0.350
sex.2	speed	0.166	0.146	1.138	0.255
school.GW	visual	-0.259	0.184	-1.404	0.160
school.GW	textual	0.521	0.129	4.053	< 0.001
school.GW	speed	-0.139	0.151	-0.922	0.357

moderate multivariate fit on the training data (overall $R^2 = 0.632$ when aggregating squared errors over all origins and destinations). The estimated projection directions typically mix the four hubs within each term (e.g., one term loads heavily on Osaka and Fukuoka while another mixes Tokyo and Aichi), so interpretability hinges on ridge-function diagnostics rather than a direct hub-to-component correspondence.

Topic model: Structural topic model (STM)

As a robustness check using an off-the-shelf probabilistic topic model, we also fitted a structural topic model (STM) with three topics using the `stm` package (Roberts et al., 2014, 2019). To mirror the NMF-RE covariate coding, we used the prevalence formula

$$\text{prevalence} = \sim 0 + \text{era},$$

so that STM estimates an era-specific expected topic prevalence level for each era (Early, Industrial, Postwar) *without an intercept*. Table G2 reports these era-level prevalence

estimates with simulation-based standard errors under global uncertainty; p-values are two-sided. Under this parameterization, small (near-zero) coefficients indicate that a topic is nearly absent in an era, which is directly comparable (qualitatively) to the “near-zero” interpretation under the NMF-RE mean-structure coding.

Because topic labels are identifiable only up to permutation, we aligned STM topics to the NMF-RE topic labels by inspecting representative words (e.g., via `labelTopics` and $\text{Pr}(\text{topic} \mid \text{word})$). In this corpus, STM Topic 2 corresponds to our Topic 1 (institutional/legal; *constitution/laws/congress*), STM Topic 3 aligns with our Topic 2 (union/constitutional/foreign; *war/union/foreign*), and STM Topic 1 corresponds to our Topic 3 (modern civic rhetoric; *today/america/freedom/world*). Accordingly, Table G2 reports STM results after relabeling topics to match the NMF-RE Topic 1–3 order.

With this alignment, STM corroborates the same qualitative historical pattern. The civic-rhetoric topic (Topic 3) increases sharply from Early to Postwar, whereas the institutional/legal topic (Topic 1) becomes small in the Postwar era. The union/foreign topic (Topic 2) declines after the Early era but remains non-negligible.

Table G2

STM era-level topic prevalence estimates for the inaugural-address corpus ($K = 3$), fitted with $\mathbf{prevalence} = \sim \mathbf{0} + \mathbf{era}$ (no intercept). Topics are relabeled to align with the NMF-RE Topic 1–3 order (STM 2→Topic 1, STM 3→Topic 2, STM 1→Topic 3). Standard errors are simulation-based under global uncertainty; p -values are two-sided.

Covariate	Topic	Estimate	SE	t	p
Early (1775–1865)	Topic 1	0.51913	0.05369	9.669	< 0.001
Early (1775–1865)	Topic 2	0.40326	0.04381	9.205	< 0.001
Early (1775–1865)	Topic 3	0.07741	0.03688	2.099	0.040
Industrial (1865–1945)	Topic 1	0.47425	0.05336	8.887	< 0.001
Industrial (1865–1945)	Topic 2	0.19953	0.04014	4.971	< 0.001
Industrial (1865–1945)	Topic 3	0.32591	0.04181	7.796	< 0.001
Postwar (1945–)	Topic 1	0.05729	0.04878	1.175	0.245
Postwar (1945–)	Topic 2	0.15039	0.04002	3.758	< 0.001
Postwar (1945–)	Topic 3	0.79233	0.04005	19.782	< 0.001

References

- Benoit, K., Watanabe, K., Wang, H., Nulty, P., Obeng, A., Müller, S., & Matsuo, A. (2018). Quanteda: An r package for the quantitative analysis of textual data. *Journal of Open Source Software*, 3(30), 774. <https://doi.org/10.21105/joss.00774>
- Bollen, K. A. (1989). *Structural equations with latent variables* (Vol. 25). Wiley.
- Breslow, N. E., & Clayton, D. G. (1993). Approximate inference in generalized linear mixed models. *Journal of the American statistical Association*, 88(421), 9–25.
- Cameron, A. C., Gelbach, J. B., & Miller, D. L. (2008). Bootstrap-based improvements for inference with clustered errors. *The review of economics and statistics*, 90(3), 414–427.
- Cemgil, A. T. (2009). Bayesian inference for nonnegative matrix factorisation models. *Computational intelligence and neuroscience*, 2009(1), 785152.
- Ding, C., Li, T., Peng, W., & Park, H. (2006). Orthogonal nonnegative matrix t-factorizations for clustering. *Proceedings of the 12th ACM SIGKDD international conference on Knowledge discovery and data mining*, 126–135.
- Efron, B. (2004). The estimation of prediction error: Covariance penalties and cross-validation. *Journal of the American Statistical Association*, 99(467), 619–632.
- Févotte, C., & Idier, J. (2011). Algorithms for nonnegative matrix factorization with the β -divergence. *Neural computation*, 23(9), 2421–2456.
- Friedman, J. H. (1984). *Smart user's guide* (tech. rep. No. 1). Laboratory for Computational Statistics, Stanford University.
<https://purl.stanford.edu/pd898dq6156>
- Friedman, J. H., & Stuetzle, W. (1981). Projection pursuit regression. *Journal of the American statistical Association*, 76(376), 817–823.
- Gillis, N. (2014). The why and how of nonnegative matrix factorization. *Regularization, optimization, kernels, and support vector machines*, 12(257), 257–291.
- Gillis, N. (2020). *Nonnegative matrix factorization*. SIAM.

- Gillis, N., & Rajkó, R. (2023). Partial identifiability for nonnegative matrix factorization. *SIAM Journal on Matrix Analysis and Applications*, *44*(1), 27–52.
- Grabski, I. N., Trippa, L., & Parmigiani, G. (2025). Bayesian multi-study non-negative matrix factorization for mutational signatures. *Genome Biology*, *26*(1), 98.
- Holzinger, K. J., & Swineford, F. (1939). A study in factor analysis: The stability of a bi-factor solution. *Supplementary educational monographs*.
- Huber, P. J., et al. (1967). The behavior of maximum likelihood estimates under nonstandard conditions. *Proceedings of the fifth Berkeley symposium on mathematical statistics and probability*, *1*(1), 221–233.
- Javanmard, A., & Montanari, A. (2014). Confidence intervals and hypothesis testing for high-dimensional regression. *The Journal of Machine Learning Research*, *15*(1), 2869–2909.
- Jöreskog, K. G. (1969). A general approach to confirmatory maximum likelihood factor analysis. *Psychometrika*, *34*(2), 183–202.
- Jöreskog, K. G., & Goldberger, A. S. (1975). Estimation of a model with multiple indicators and multiple causes of a single latent variable. *Journal of the American statistical Association*, *70*(351a), 631–639.
- Kenward, M. G., & Roger, J. H. (1997). Small sample inference for fixed effects from restricted maximum likelihood. *Biometrics*, 983–997.
- Laird, N. M., & Ware, J. H. (1982). Random-effects models for longitudinal data. *Biometrics*, 963–974.
- Lee, D., & Seung, H. S. (2000). Algorithms for non-negative matrix factorization. In T. Leen, T. Dietterich, & V. Tresp (Eds.), *Advances in neural information processing systems* (Vol. 13). MIT Press. https://proceedings.neurips.cc/paper_files/paper/2000/file/f9d1152547c0bde01830b7e8bd60024c-Paper.pdf
- Lee, D. D., & Seung, H. S. (1999). Learning the parts of objects by non-negative matrix factorization. *Nature*, *401*(6755), 788–791.

- Mammen, E. (1993). Bootstrap and wild bootstrap for high dimensional linear models. *The annals of statistics*, 21(1), 255–285.
- Ministry of Land, Infrastructure, Transport and Tourism. (2021). National road traffic census: Origin–destination tables between prefectures [Accessed: 2026-01-10]. https://www.e-stat.go.jp/stat-search/files?stat_infid=000040170612
- Phelan, G., & Campbell, D. A. (2025). Testing hypotheses of covariate effects on topics of discourse. *arXiv preprint arXiv:2506.05570*.
- Pinheiro, J., Bates, D., & R Core Team. (2025). *Nlme: Linear and nonlinear mixed effects models* [R package version 3.1-168]. <https://doi.org/10.32614/CRAN.package.nlme>
- Potthoff, R. F., & Roy, S. N. (1964). A generalized multivariate analysis of variance model useful especially for growth curve problems. *Biometrika*, 51, 313–326.
- Roberts, M. E., Stewart, B. M., & Tingley, D. (2019). Stm: An r package for structural topic models. *Journal of Statistical Software*, 91, 1–40.
- Roberts, M. E., Stewart, B. M., Tingley, D., Lucas, C., Leder-Luis, J., Gadarian, S. K., Albertson, B., & Rand, D. G. (2014). Structural topic models for open-ended survey responses. *American journal of political science*, 58(4), 1064–1082.
- Robinson, W., Sharan, R., & Leiserson, M. D. (2019). Modeling clinical and molecular covariates of mutational process activity in cancer. *Bioinformatics*, 35(14), i492–i500.
- Rosales, R. A., Drummond, R. D., Valieris, R., Dias-Neto, E., & Da Silva, I. T. (2017). Signer: An empirical bayesian approach to mutational signature discovery. *Bioinformatics*, 33(1), 8–16.
- Rosseel, Y. (2012). Lavaan: An r package for structural equation modeling. *Journal of statistical software*, 48(1), 1–36.
- Satoh, K. (2023). On non-negative matrix factorization using gaussian kernels as covariates [in Japanese]. *Japanese Journal of Applied Statistics*, 52(2), 59–74.

- Satoh, K. (2025). *Nmfkc: Non-negative matrix factorization with covariates and structural extensions* [R package version 0.5.8]. <https://ksatohds.github.io/nmfkc/>
- Satoh, K., & Yanagihara, H. (2010). Estimation of varying coefficients for a growth curve model. *American Journal of Mathematical and Management Sciences*, *30*(3-4), 243–256.
- Schmidt, M. N., Winther, O., & Hansen, L. K. (2009). Bayesian non-negative matrix factorization. *International Conference on Independent Component Analysis and Signal Separation*, 540–547.
- Taylor, J., & Tibshirani, R. J. (2015). Statistical learning and selective inference. *Proceedings of the National Academy of Sciences*, *112*(25), 7629–7634.
- Tibshirani, R. J., & Taylor, J. (2012). Degrees of freedom in lasso problems. *The Annals of Statistics*, *40*(2), 1198–1232. <https://doi.org/10.1214/12-AOS1003>
- van de Geer, S., Bühlmann, P., Ritov, Y., & Dezeure, R. (2014). On asymptotically optimal confidence regions and tests for high-dimensional models. *The Annals of Statistics*, *42*(3), 1166–1202. <https://doi.org/10.1214/14-AOS1221>
- Vonesh, E. F., & Carter, R. L. (1987). Efficient inference for random-coefficient growth curve models with unbalanced data. *Biometrics*, 617–628.
- White, H. (1980). A heteroskedasticity-consistent covariance matrix estimator and a direct test for heteroskedasticity. *Econometrica: journal of the Econometric Society*, 817–838.